UNCERTAINTY ANALYSIS IN LATTICE PHYSICS CALCULATIONS

APPLICATION OF THE NRG's TALYS EVALUATED DATA TO A CASE OF BURNUP

Francisco Ferragut Ferretjans

SUPERVISORS:

Pouya SABOURI
Adrien BIDAUD

DISSERTATION COMMITTEE:

Grégoire KESSEDJIAN

Alexis NUTTIN

Remerciements

Il faut remercier en premier lieu Pouya Sabouri de m'avoir reçu et d'avoir accepté d'être mon tuteur. Il a réussi à me montrer la physique tout aussi bien au laboratoire qu'au bar..., avec de la patience et du copinage, il a toujours trouvé le temps pour répondre à mes questions et à mes problèmes. Vraiment, plus qu'un tuteur il est devenu un grand ami. Merci beaucoup.

Je ne peux pas oublier Henry-Emmanuel Thyébault, non seulement pour la puissance de son serveur, sans laquelle il n'aurait pas été possible de faire tout ce travail, mais aussi pour les corrections avec le français et, de sûrcroit, pour l'appui qu'il m'a donné en tout temps.

Merci également à Shahab Dabiran (CANDU ENERGY INC.) qui, avec ses vastes connaissances dans DRAGON, m'a permis d'obtenir des bons résultats. Sans lui, tout cela n'aurait pas été possible. Un grand merci également au Dr. D. Rochman (NRG), pour avoir fourni les fichiers qui ont été la base de mes travaux et pour son intérêt ainsi que ses réponses par courrier électronique.

Enfin, à Adrien Bidaud, pour m'avoir acceuilli, pour sa patience et l'aide dans la difficile tâche d'interpréter les résultats du Burnup.

En général, grâce à tous ceux qui ont rendu mon séjour dans ce laboratoire inoubliable.

Contents

Remerciements **1**

1 Introduction **6**
1.1 Overview of the Nuclear Data File 7
1.2 TALYS generated Nuclear Data Files 9
1.3 Multigroup Cross Sections 11

2 Steady State Problems **14**
2.1 Elements of Sensitivity and Uncertainty Analysis 14
2.2 k_{eff} Sensitivities 15
2.3 Comparison of the TALYS uncertainties with JENDL-4 and SCALE 6 17

3 Burnup **24**
3.1 Definitions 24
3.1.1 Isotopic Densities 24
3.1.2 Flux Uncertainties 25
3.1.3 Isotopic Mass Changes 26
3.2 Uncertainties of ^{235}U Density 27
3.2.1 Uncertainties due to variations in the cross sections of ^{235}U 28
3.2.2 Uncertainties due to variations in the cross sections of ^{238}U 30
3.2.3 Uncertainties due to variations in the cross sections of ^{239}Pu 30
3.3 Uncertainties of ^{238}U Density 31
3.3.1 Uncertainties due to variations in the cross sections of ^{235}U 32
3.3.2 Uncertainties due to variations in the cross sections of ^{238}U 33
3.4 Uncertainties of ^{239}Pu 34
3.4.1 Uncertainties due to variations in the cross sections of ^{238}U 35
3.4.2 Uncertainties due to variations in the cross sections of ^{239}Pu 37
3.4.3 Uncertainties due to variations in the cross sections of ^{235}U 37

4 Final Remarks **39**

A Comparison of uncertainties between TALYS, JENDL-4 & SCALE **42**
A.1 Comparison of the Uncertainties from JENDL-4,SCALE and TALYS 42
A.1.1 ^{238}U cross section uncertainties for the TALYS generated covariances . . 42
A.1.2 ^{238}U cross section uncertainties for the TALYS generated covariances . . 44
A.1.3 Correlation matrices 46

B Input NJOY **54**

C Validation for WIMSR.PY and WIMSLIB.py **55**

List of Figures

1.1 Parameters efects in a SLBW resonance . . . 8
1.2 Parameters efects in a SLBW scattering resonance . . . 9
1.3 Random parameters used for reconstruction of resolved ressonances for U^{238} . . . 10
1.4 Influence of the random parameters in the first Peak from PU^{239} . . . 11
1.5 NJOY flow chart . . . 11
1.6 Coupling of the NRG data with the transport code (DRAGON) . . . 12
1.7 Random Multigroup Σ_T cross sections for ^{238}U . . . 13
1.8 Random Integral resonances for ^{238}U at group 65 . . . 13

2.1 Flow chart for Sensitivity and Uncertainty calculations . . . 16
2.2 Inputs of *covbuild.py* . . . 18
2.3 Resultant variations of k_{eff} from cross section uncertainties of ^{235}U . . . 19
2.4 Resultant variations of k_{eff} from cross section uncertainties of ^{238}U . . . 19
2.5 Comparison of the fission cross section uncertainty between the TALYS generated covariances, SCALE-6, and JENDL-4 covariances . . . 21
2.6 Comparison of the ^{238}U $\bar{\nu}$ uncertainty between the TALYS generated covariances, SCALE-6, and JENDL-4 covariances . . . 23

3.1 Isotopic fission contribution with time . . . 26
3.2 Example of flux evolution due to Plutonium buildup . . . 26
3.3 Production and decay for the most important isotopes in the UAM Benchmark . 27
3.4 U^{235} density evolution due to cross section uncertainties of U^{235},U^{238},Pu^{239} and Pu^{241} . . . 28
3.5 Evolution of the flux ϕ, density N^{235} and density change ΔN^{235} due to uncertainties of ^{235}U . . . 29
3.6 Uncertainty evolution as a result of the uncertainties of ^{238}U . . . 30
3.7 Uncertainty evolution as a result of the uncertainties of ^{239}Pu . . . 31
3.8 U^{238} density by cross section changes in U^{235},U^{238},Pu^{239} and Pu^{241} . . . 32
3.9 Uncertainty evolution as a result of the uncertainties of ^{235}U . . . 33
3.10 Uncertainty evolution as a result of the uncertainties of ^{238}U . . . 33
3.11 ^{238}U capture cross section over the time . . . 34
3.12 Pu^{239} density evolution due to cross section variations in U^{235},U^{238},Pu^{239} and Pu^{241} . . . 35
3.13 Negative correlation between ^{239}Pu density and ^{238}U density . . . 36
3.14 Relative uncertainity in ϕ and ^{239}Pu due at ^{238}U . . . 37
3.15 Relative uncertainity in ϕ and ^{239}Pu density due to ^{239}Pu cross section uncertainties . . . 37
3.16 Relative uncertainity in ϕ and ^{239}Pu due at ^{235}U . . . 38

A.1 ^{238}U fission cross section uncertainty for the TALYS generated covariances . . . 42

A.2 ^{238}U nubar uncertainty for the TALYS generated covariances, covariances of SCALE-6, and JENDL-4 . . . 43
A.3 ^{238}U capture cross section uncertainty for the TALYS generated covariances, covariances of SCALE-6, and JENDL-4 . . . 43
A.4 ^{238}U elastic cross section uncertainty for the TALYS generated covariances, covariances of SCALE-6, and JENDL-4 . . . 44
A.5 ^{235}U $\bar{\nu}$ uncertainties for the TALYS generated covariances, covariances of SCALE-6, and JENDL-4 . . . 44
A.6 ^{235}U fission cross section uncertainty for the TALYS generated covariances, covariances of SCALE-6, and JENDL-4 . . . 45
A.7 ^{235}U capture cross section uncertainty for the TALYS generated covariances, covariances of SCALE-6, and JENDL-4 . . . 45
A.8 ^{235}U elastic cross section uncertainty for the TALYS generated covariances, covariances of SCALE-6, and JENDL-4 . . . 46
A.9 Correlation matrix for ^{238}U TALYS for capture . . . 46
A.10 Correlation matrix for ^{238}U TALYS elastic . . . 47
A.11 Correlation matrix for ^{238}U SCALE capture . . . 47
A.12 Correlation matrix for ^{238}U SCALE elastic . . . 48
A.13 Correlation matrix for ^{238}U JENDL-4 elastic . . . 48
A.14 Correlation matrix for ^{235}U TALYS for capture . . . 49
A.15 Correlation matrix for ^{235}U TALYS elastic . . . 49
A.16 Correlation matrix for ^{235}U TALYS fission . . . 50
A.17 Correlation matrix for ^{235}U SCALE for capture . . . 50
A.18 Correlation matrix for ^{235}U SCALE elastic . . . 51
A.19 Correlation matrix for ^{235}U SCALE fission . . . 51
A.20 Correlation matrix for ^{235}U JENDL-4 for capture . . . 52
A.21 Correlation matrix for ^{235}U JENDL-4 elastic . . . 52
A.22 Correlation matrix for ^{235}U JENDL-4 fission . . . 53

List of Tables

2.1 Sensitivities for ^{238}U and ^{235}U 17
2.2 Absolute covariance contributions (in **bold**) and percentage contribution (in parenthesis) for ^{235}U from our matrices generated by *covbuild.py* and the TALYS data 20
2.3 Absolute covariance contributions (in **bold**) and percentage contribution (in parenthesis) for ^{235}U from the covariance matrices of SCALE-6 20
2.4 Absolute covariance contributions (in **bold**) and percentage contribution (in parenthesis) for ^{238}U from our matrices generated by *covbuild.py* and the TALYS data 21
2.5 Absolute covariance contributions (in **bold**) and percentage contribution (in parenthesis) for ^{238}U from the covariance matrices of JENDL-4 22
2.6 Absolute covariance contributions (in **bold**) and percentage contribution (in parenthesis) for ^{238}U from the covariance matrices of SCALE 6 22

C.1 K_{eff} and error for the isotopes studied 56

Chapter 1

Introduction

The basis of any physics computation in nuclear engineering is experimental data often treated through some form of evaluation to prepare use for the engineer or physicist. In reactor physics, where one is involved with the behavior of the neutron population across the reactor core, the data of interest is the neutron cross section (interaction probability) for the various isotopes appearing in the reactor core. Such data is arrived at through the evaluation of experimentally measured parameters with the application of various theoretical nuclear models and empirical formulations along the way. The evaluation results in what is called an Evaluated Nuclear Data File (ENDF) which containing various cross section parameters which can be used to describe the possible interactions of interest (such as fission and spectrum of fission particles, capture, elastic and inelastic scattering, (n,2n),etc. reactions) with the target nuclei.

A number of such evaluations include the North American ENDF[1][1], the European JEFF[2][2], the Japanese JENDL[3] [3] as well as the Dutch TENDL [4] evaluations.

With a proper processing of the ENDF file, one can arrive at a multi-group cross section library which may be used for deterministic transport calculations. The question of interest in this report is how the uncertainties originating from the experimental data and models used in the evaluation affect the accuracy of calculations performed by the transport code. The effort is delicate for a number of reasons; First, the notion of including such cross section uncertainties is still in the developmental phase [5]. Next, the task of producing usable data for the transport code is arduous involving many calculations along the way. Finally, once uncertainties are propagated, due to the complexity of the physics involved, the task of interpreting the data and providing valuable feedback is quite challenging. As a case study, the base data that we have chosen is that produced by Nuclear Research Consultancy Group (NRG) by their use of the TALYS [4] code. From their data, we generate a random set of mult-igroup cross section libraries which may be used to perform the act of uncertainty propagation in transport calculations. A benefit of this choice is that the uncertainty propagation is started at the most elementary step after the evaluation-the evaluated nuclear data file. This eliminates the idea of discontinuous cross sections which would arise had the propagation been started at a later step in the calculation[5] [6]. Chapter 2 of this work provides a survey of the NRG data through application to a case of criticality safety assessment. In Chapter 3, we provide results made possible by the tools

[1] `http://www.nndc.bnl.gov/exfor/endfb7.1.jsp`

[2] `http://www.oecd-nea.org/dbforms/data/eva/evatapes/jeff_31/`

[3] `http://wwwndc.jaea.go.jp/jendl/j40/j40.html`

[4] `ftp://ftp.nrg.eu/pub/www/talys/tendl2011/tendl2011.html`

[5] we note at passing that at the time of the writing of this work, of the mentioned evaluations above the JENDL, ENDFBVII.1 and TENDL are the only evaluations containing covariance data

developed in the course of this work which allow the application of the generated libraries to a case of burnup using the Total Monte Carlo approach. A similar application using MCNP and the burnup code Serpent is already available and has been discussed elsewhere[7], [15].

1.1 Overview of the Nuclear Data File

The backbone of any physics calculation is the nuclear data file. The data file contains a vast amount of information regarding the behaviour of the various reaction cross sections over a large span of energy (usually starting at 10^{-5} eV and ending at $> 10^7$ eV). To condense the necessary space required for the representation of the cross section , the ENDF-BVI [8] format is often used allowing for various interpolation laws (log-log, log-lin, lin-lin, lin-log, constant-lin and constant-log) over different energy ranges. The ENDF file is organized into different sections (called tapes) containing various cross section parameters.

For heavy isotopes which are dominated by resonances in the epithermal range, the nuclear data file contains various resonance parameters with an associated formalism (Single Level Breit-Wigner, Multi Level Breit-Wigner, Reich-Moore, etc) from which the cross section may be constructed. These parameters vary based on the type of the resonance (scattering, absorption, fission) as well as the formalism used to represent the resonance. As the parameters are arrived at through the evaluation of experimental results, an associated uncertainty is accompanied with them[6].

For the general capture (n, γ) reactions where a compound nucleus is formed by the absorption of a neutron n with successive decay by of a γ emission, a resonance at energy E_{res} may be represented using the Sigle Level Breit Weigner Formula as:

$$\sigma_{n,\gamma} = 4\pi\lambda^2 g\frac{\Gamma_n}{\Gamma} * \frac{\Gamma_\gamma}{\Gamma}\frac{1}{\frac{4}{\Gamma^2}(E - E_{res})^2 + 1} = \sigma_{n,b} = \sigma_0\frac{\Gamma_\gamma\Gamma_n}{\Gamma^2}\frac{1}{1+y^2} \tag{1.1}$$

where $y = \frac{2(E-E_{res})}{\Gamma}$, g is the statistical spin factor accounting for the possible spin vector combinations of the neutron and the target nucleus, Γ_n, Γ_γ and Γ represents the neutron scattering, radiative and total widths of the resonance. From equation 1.1, one can see that an uncertainty in the E_{res} results in a horizontal shift of the position of the resonance while uncertainties in the resonance width result a widening or thinning of the resonance. Figure 1.1 describes the variation of the resonance capture resonance of ^{239}Pu for various factors of the resonance width Γ_γ and Γ .

[6] If the evaluation contains covariance data, these uncertainties are reported in tapes 31-35

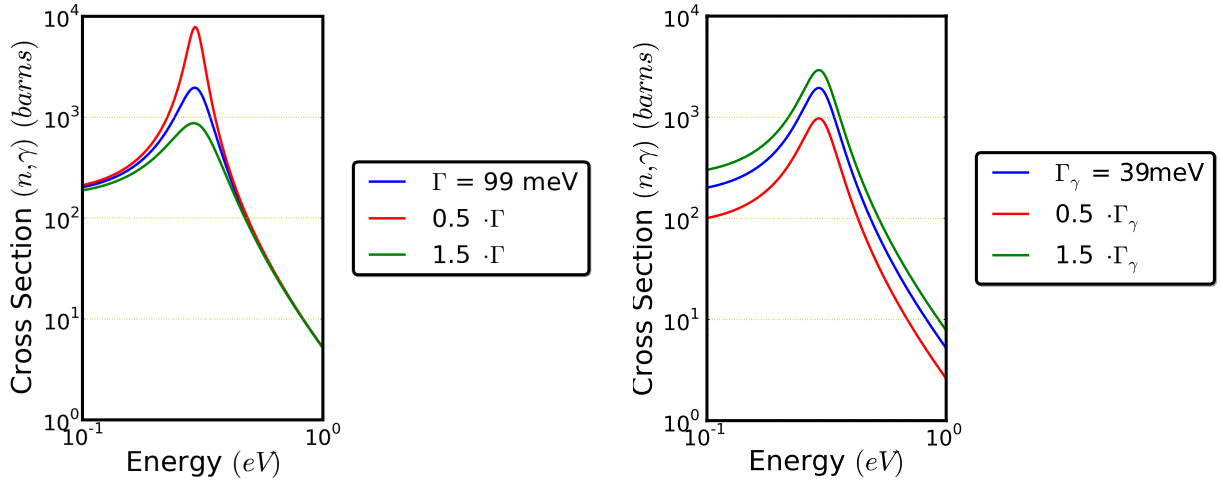

Figure 1.1: Parameters efects in a SLBW resonance
^{239}Pu Resonance at 0.295 eV. $\Gamma = 99$ meV, Γ_n =0.134 meV, $\Gamma_\gamma = 39$ meV and J=1 [9]

In the case of elastic scattering, the description of the resonance is more complicated. Using the Breit Wigner formalism, the cross section may be expressed as a sum of three terms; the first term accounting for the background/potential scattering σ_0, the second term proportional to $\frac{\Gamma_n\Gamma}{(E-E_0)^2+\frac{1}{4}\Gamma^2}$ describing the symmetric form of the resonance, along with a third term describing the interference between the resonance and the background/potential cross section.

$$\sigma_s = 4\pi R^2 + [\sigma_0\frac{\Gamma_n}{\Gamma} + \frac{\sigma_0 2Ry}{\lambda}]\frac{1}{1+y^2} \tag{1.2}$$

Figure 1.2 describes variation in the resonances of ^{239}Pu at energy 0.295 eV for various values of the parameters seen in equation 1.2

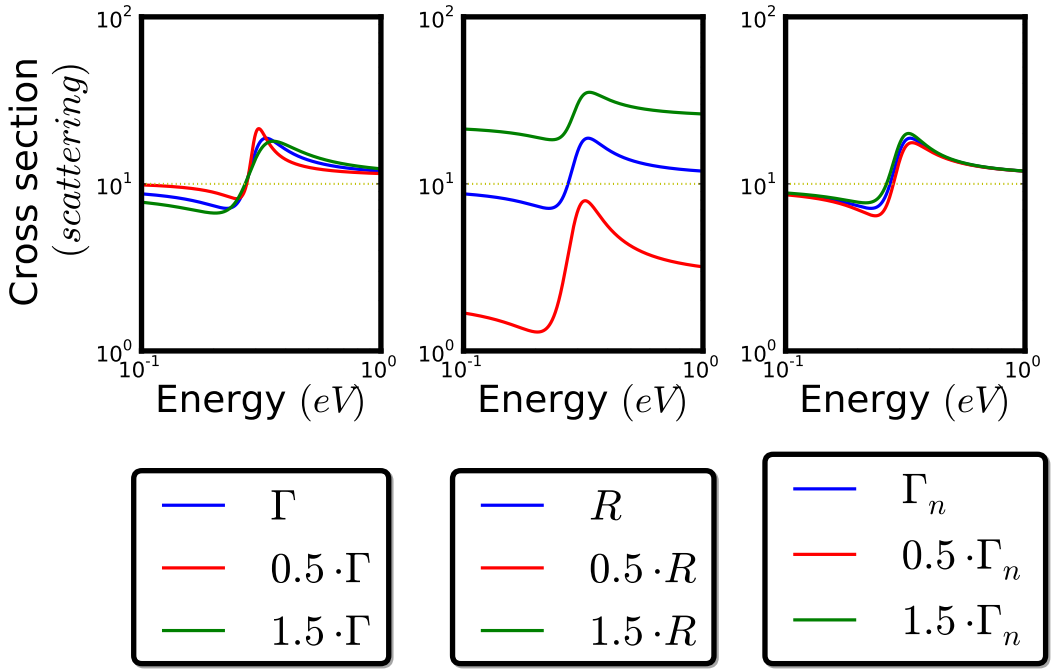

Figure 1.2: Parameters efects in a SLBW scattering resonance
^{239}Pu scattering resonance at 0.295 eV, with $\Gamma = 99$ meV, Γ_n =0.134 meV [9]and R =0.941 [10]

At higher energies the resonances become too close to one another to be distinguishable through experimental measurements. Therefore, the formalism used in this range is that of average values [11] calculated by a best fit of the experimental data. As one increases to higher energies (for major actinides-larger than a few keV), several additional forms of interaction (inelastic scattering, $(n, 2n)$, (n, α), etc) become possible. Figure ... shows the general threshold reactions for ^{238}U.

1.2 TALYS generated Nuclear Data Files

The base data used in this work is the data provided [7] by the Nuclear Research and Consultancy Group (NRG). NRG has developed a Monte Carlo method for nuclear data uncertainty propagation [12] which can be used to study the impact of nuclear data uncertainties in physics calculations. Figure 1.3 presents the variation in the resonance scattering width, Γ_γ, capture width, Γ_n, and fission channels Γ_{Fa}, and Γ_{Fb}, over the resolved resonance range as reported in the random nuclear data files.

[7] `ftp://ftp.nrg.eu/pub/www/talys/random/random.html`

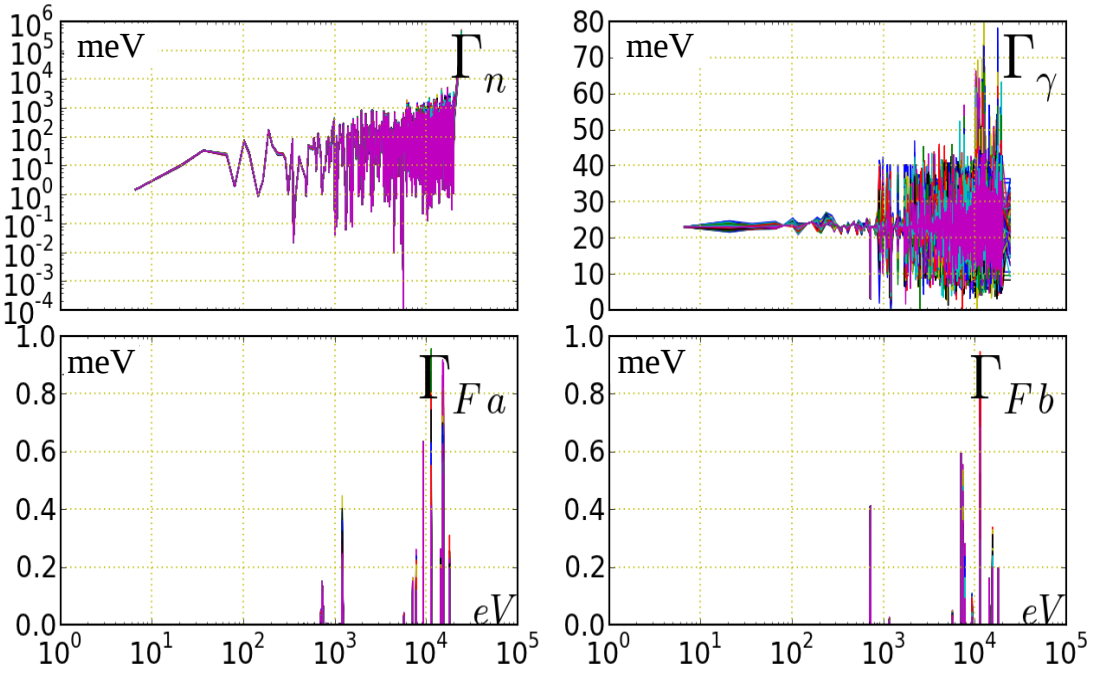

Figure 1.3: Random parameters used for reconstruction of resolved ressonances for U^{238}

The parameters presented in the figure above are generated by NRG using the TALYS code. The TALYS code is used to generate all the necessary information for the nuclear data file (input values of the TALYS code are produced using other codes as TASMAN, TEFAL, TARES, and TANES). By running TALYS several times, each time with a different samples of the TALYS input parameters, the NRG team generates a random sample of possible nuclear data files. The effect of the resulting variations are provided for the first resonance of ^{239}Pu which appears at 0.295 eV. Naturally, the quality of the results depend greatly on the source of the uncertainties and the covariances used. The cross section parameter uncertainties used by the TALYS code are directly taken from the EXFOR [8] data base [14] Additionally, the input parameters of the TALYS code are assumed to vary independently [15]. This may result in a higher spread[15] (than what is expected in comparison to available covariance data) in parameter uncertainties with parameter correlations differing from those currently available in other covariance sources.

[8] `http://www.nndc.bnl.gov/exfor/exfor00.htm`

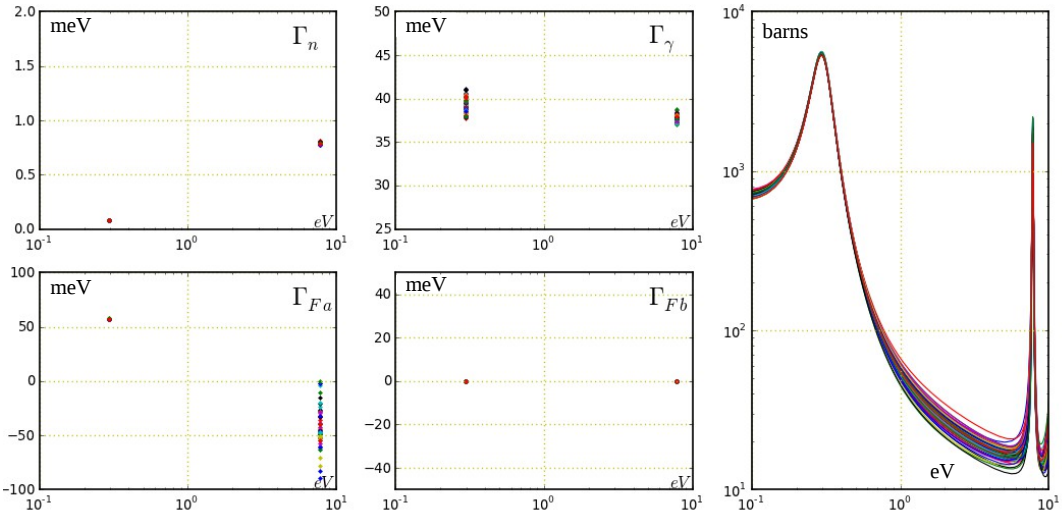

Figure 1.4: Influence of the random parameters in the first Peak from PU^{239}

1.3 Multigroup Cross Sections

Before the cross section data can used by a transport code such as DRAGON, the data must be processed by a nuclear data processing code. The NJOY [16] code is used in this report for this purpose. The library format we have chosen in this work is that of the 172 group WIMS-D4 [17] format provided by the IAEA.

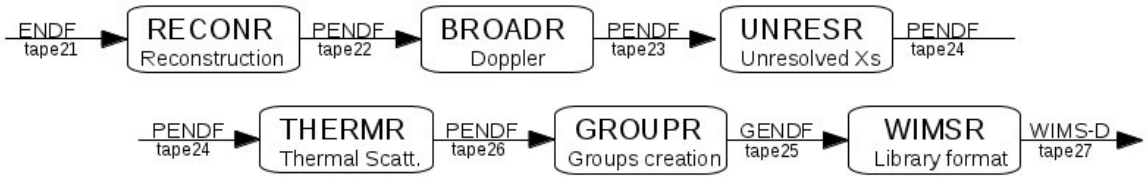

Figure 1.5: NJOY flow chart

Figure 1.5 shows the flow chart for the NJOY models used in the the library creation process. The NJOY program has a modular approach with the output of each module (called an NJOY tape) being an input for the next. The RECONR module of NJOY is used to represent the cross section data in continuous energy form for the temperatures available on the evaluated file. The BROADR module is used to perform Doppler broadening of the resonances for a number of demanded temperatures. The UNRESR module produces cross section values for the unresolved resonance region as a function of a background moderator cross section which is provided by the user as an input parameter. The GROUPR module is used to calculate the slowing down flux as a function of the various background moderator cross sections. This flux is subsequently used as a weighting flux to produce multi-group cross section. Finally, the WIMSR module provides tabulated cross sections as functions of temperature and background moderator

cross section (dilution factors) for the lumped reactions of "absorption", "scattering" and fission (where present). At this stage, the definition of the cross section is quite different than that in the nuclear data file. In particular, scattering matrix $\hat{S} = (S)_{gg'}$ is defined defined as [17]:

$$S_{gg'} = \sigma_{elastic}^{g \to g'} + \sum_i \sigma_{inelastic^i}^{g \to g'} + 2 * \sigma_{(n,2n)}^{g \to g'} + 3 * \sigma_{(n,3n)}^{g \to g'} \tag{1.3}$$

where i varies over the available inelastic levels of the isotope in question. The scattering cross section $\sigma_{SCAT}^{g} = \sum_{g'} S_{gg'}$ is defined as the sum over the outgoing group g'. To preserve neutron balance, an "absorption" cross section is defined as the sum of all reactions resulting in capture, subtracted by:

$$\sigma_{ABS} = \sum_{x \in (n,\gamma),(n,\alpha),(n,p),..} \sigma_x - \sigma_{(n,2n)} - 2 * \sigma_{(n,3n)} \tag{1.4}$$

For each random file, the illustrated modules of NJOY are ran to arrive at a final wimsr tape. Then, the data corresponding to the isotope in question in the **jeff31gx** library is replaced by that originating from the random file. Two main programs (wimsr.py and wimslib.py) have been written in PYTHON which allow for the easy manipulation of the WIMS libraries. For each created library a simulation can be performed by the transport code as shown in figure 1.6. Approximately a few hundred evaluated data files provided by NRG were processed for each of the isotopes: U_{235}, U_{238}, Pu_{239}, and Pu_{242}. The Pu_{240} files were found to be corrupt and NRG has been notified of the problem[9].

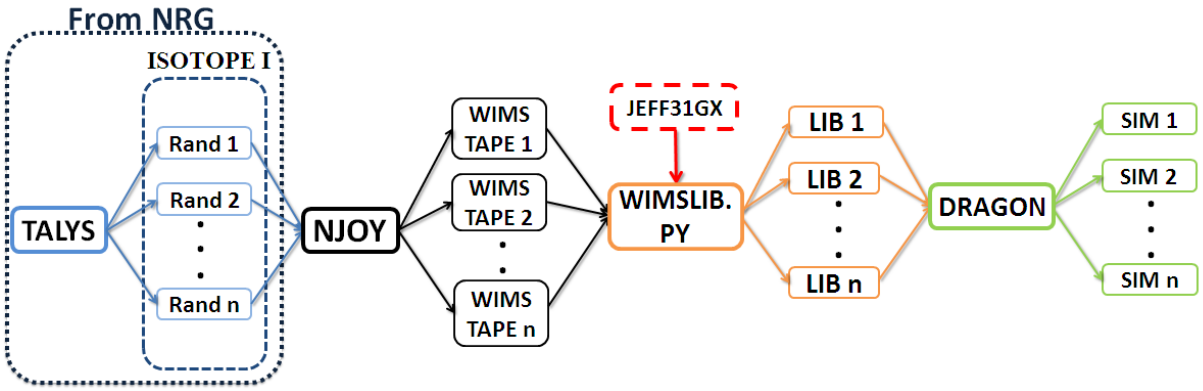

Figure 1.6: Coupling of the NRG data with the transport code (DRAGON)

Figure 1.7 presents a sample of the total cross section of ^{238}U at infinite dilution generated from the NRG data, along with the cross section obtained from the JEFF 3.1 evaluation (red).

[9] correspondence with Dr. D. Rochman

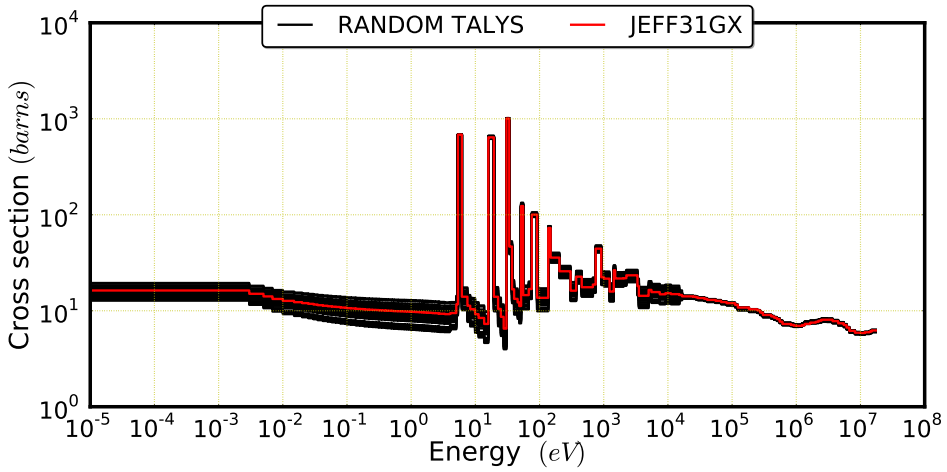

Figure 1.7: Random Multigroup Σ_T cross sections for ^{238}U

As mentioned earlier, the cross section is presented in the library in tabulated form as a function of temperature and dilution. In the transport calculation, for the heavy isotopes where self shielding effects are important, an "equivalent" [18] geometry dependent dilution factor is calculated for each group. The cross section at the equivalent dilution factor is obtained by interpolating over the "resonance integral"[17]. Figure 1.8 presents the resonance integral of ^{238}U at Group 65(136 eV to 147eV).

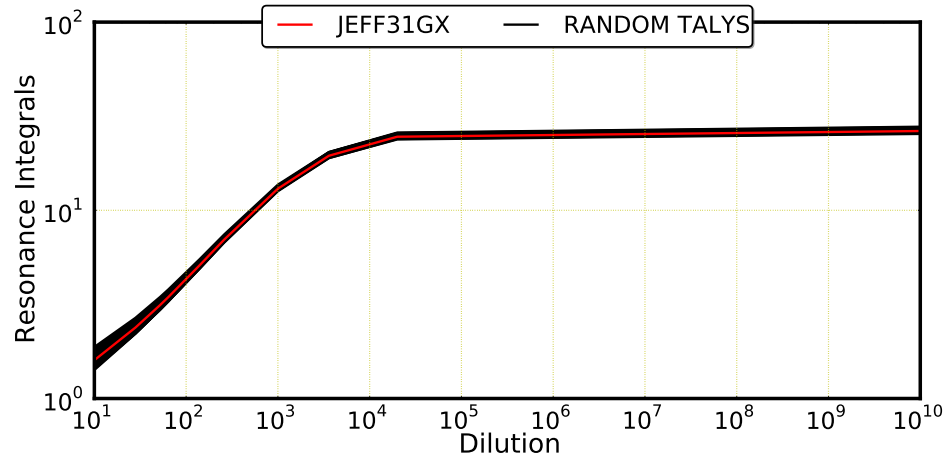

Figure 1.8: Random Integral resonances for ^{238}U at group 65

Chapter 2

Steady State Problems

As discussed in chapter 1, the cross section parameter uncertainties and correlations by which the random set of nuclear data files have been produced may result in an over estimation of the predicted uncertainties of the various reactions. In this chapter, we provide a comparison between the multi-group cross section uncertainties and correlations based on the TALYS generated random files and the cross section uncertainties and correlations which already exist in JENDL-4 and SCALE-6. The uncertainty results are provided for the PWR cell described in the OECD UAM Phase I report[19]. The code used for the transport calculation is the DRAGON code[20] developed at the Ecole Polytechnique de Montreal. For the sensitivity analysis, we have used our code[1] written in PYTHON that uses classical perturbation theory to calculate reaction sensitivities[2].

2.1 Elements of Sensitivity and Uncertainty Analysis

Given n observations of the vectors $\bar{\sigma}_x \in \mathbb{R}^m$, $\bar{\sigma}_y \in \mathbb{R}^m$ generated from the observables $\bar{\sigma_x} = (\sigma_x^g)_{g=1,..,m}$ and $\bar{\sigma_y} = (\sigma_y^g)_{g=1,..,m}$, we define the relative covariance matrix $COV(\bar{\sigma}_x, \bar{\sigma}_y) \in \mathbb{R}^{m\times m}$ generated by elements $COV(\sigma_x, \sigma_y)_{g,g'}$ as:

$$COV(\bar{\sigma}_x, \bar{\sigma}_y)_{g,g'} = \frac{\mathbb{E}[(\sigma_x^g - \bar{\sigma}_x^g)(\sigma_y^g - \bar{\sigma}_y^{g'})]}{\bar{\sigma}_x^g \bar{\sigma}_y^{g'}} \tag{2.1}$$

where we have used the symbol $\mathbb{E}[x]$ to represent the expectation value x, and $\bar{\sigma}_x^g$ and $\bar{\sigma}_y^g$ to represent the average value for the n observations.
Furthermore, given a function $R(\bar{\sigma}_{x_1}, \bar{\sigma}_{x_2}, ..., \bar{\sigma}_{x_k}) \in \mathbb{R}$ of the vector parameters $\bar{\sigma}_{x_{i=1,..,k}}$, we define the sensitivity vector $\bar{S}_{\bar{\sigma}_x} \in \mathbb{R}^m$ as:

$$\bar{S}_{\bar{\sigma}_{x_l}} = \frac{\bar{\sigma}_x}{R} \frac{\partial R}{\partial \bar{\sigma}_{x_l}} \tag{2.2}$$

As can be seen from the above equation, the sensitivity coefficient $S_{\bar{\sigma}_{x_l}}$ is just the first term in the Taylor expansion of the function $R(\bar{\sigma}_{x_1}, \bar{\sigma}_{x_2}, ..., \bar{\sigma}_{x_k}) \in \mathbb{R}$ about the point $\bar{\sigma}_{x_l} \in \mathbb{R}^m$. The coefficient $\frac{\bar{\sigma}_x}{R}$ in equation 2.2 acts as a normalization factor so that the sensitivity $S_{\bar{\sigma}_{x_l}}$ (%/%) is the expected relative change (%) in the value of the function R resultant from a perturbation

[1] Note that the first part of this internship contributed to the generation of libraries as well as some of the modules used by our code

[2] This chapter has been written in collaboration with P. Sabouri

(%) in the values of the vector $\bar{\sigma}_{x_l}$.
Given the matrix $\mathbf{M} \in \mathbb{R}^{(m\times k)\times(m\times k)}$ containing the $k\times k$ block matrices $\mathbf{M}_{j,l=1,..,m} = COV(\bar{\sigma}_{x_j}, \bar{\sigma}_{x_l})$ defined by equation 2.1, the relative uncertainty σ_R (in %) of $R(\bar{\sigma}_{x_1}, \bar{\sigma}_{x_2}, ..., \bar{\sigma}_{x_k})$ resulting from the uncertainties of the vectors $\bar{\sigma}_{x_{i=1,..,k}}$ can be calculated up to first order by the well known [21] sandwich formula:

$$\sigma_R^2 = \sum_{j=1}^{k}\sum_{l=1}^{k} \bar{S}_{\bar{\sigma}_{x_l}} \mathbf{M}_{lj} \bar{S}^{\dagger}_{\bar{\sigma}_{x_j}} \tag{2.3}$$

where † represents matrix transposition.

2.2 k_{eff} Sensitivities

Given the Boltzmann transport equation and its adjoint in multi-group form:

$$-\bar{\Omega}\cdot\nabla\bar{\phi} + \sum_I N_I \bar{\sigma}_{T,I}\cdot\bar{\phi} = \sum_I N_I \hat{S}_I \bar{\phi} + \frac{1}{k}\sum_I N_I \hat{F}_I \bar{\phi} \tag{2.4}$$

$$\bar{\Omega}\cdot\nabla\bar{\phi}^{\dagger} + \sum_I N_I \bar{\sigma}^{\dagger}_{T,I}\cdot\bar{\phi}^{\dagger} = \sum_I N_I \hat{S}^{\dagger}_I \bar{\phi}^{\dagger} + \frac{1}{k}\sum_I N_I \hat{F}^{\dagger}_I \bar{\phi}^{\dagger} \tag{2.5}$$

where $\bar{\phi} \in \mathbb{R}^{V\times G}$ and $\bar{\phi}^{\dagger} \in \mathbb{R}^{V\times G}$ are the forward and adjoint flux of dimensions $V \times G$ with V being the number of volumes in the geometry, G the number of energy groups, I ranging over the isotopes present in the geometry, the total cross section operator $\sigma^{gg'}_{T,I} = (\{\sigma^{g}_{SCAT,I} + \sigma^{g}_{ABS,I}\}\delta_{gg'})$, with σ^{g}_{SCAT}, σ^{g}_{ABS}, $\hat{S}$ refering to the absorption cross section, scattering cross section, and the scattering matrix defined in section 1.3, and the fission operator $F^{gg'}_I = \chi^{g'}_I \bar{\nu}^{g}_I \sigma^{g}_{I,f}$ where $\chi^{g'}_I$ is the multi-group form of the secondary energy distribution released during fission, and $\bar{\nu}^{g}_I$, and $\sigma_{I,f}$ are the total number of neutrons released per fission and the fission cross section respectively.
Ignoring feedback effects from self shielding (implicit effects), the change in the eigenvalue $\frac{1}{k}$ due to a change in the cross section $\bar{\sigma}_x \to \bar{\sigma}_x + \delta\bar{\sigma}_x$ for $x \in \{(n,n),(n,n'),(n,\alpha),(n,n\alpha),(n,p),(n,f),...\}$:

$$\bar{\sigma}_{T,I} \to \bar{\sigma}_{T,I} + \frac{\partial\bar{\sigma}_{T,I}}{\partial\bar{\sigma}_x}\delta\bar{\sigma}_x$$

$$\hat{F}_I \to \hat{F}_I + \frac{\partial\hat{F}_I}{\partial\bar{\sigma}_x}\delta\bar{\sigma}_x$$

$$\hat{S}_I \to \hat{S}_I + \frac{\partial\hat{S}_I}{\partial\bar{\sigma}_x}\delta\bar{\sigma}_x$$

may be calculated to first order by [22]:

$$\frac{\delta k}{k} = \frac{-kN_I\{\bar{\phi}^{\dagger}\frac{\partial\bar{\sigma}_{T,I}}{\partial\bar{\sigma}_{x,I}}\delta\bar{\sigma}_x\bar{\phi}\} + kN_I\{\bar{\phi}^{\dagger}\delta\bar{\sigma}_{x,I}\frac{\partial\hat{S}_I}{\partial\bar{\sigma}_x}\delta\bar{\sigma}_{x,I}\bar{\phi}\} + N_I\{\bar{\phi}^{\dagger}\frac{\partial\hat{F}_I}{\partial\bar{\sigma}_{x,I}}\delta\bar{\sigma}_{x,I}\bar{\phi}\}}{\sum_{J\in fissile} N_J\{\bar{\phi}^{\dagger}\hat{F}_J\bar{\phi}\}} \tag{2.6}$$

From equations 2.6 and 2.2 we can define the sensitivity coefficient $\bar{S}_{\bar{\sigma}_{x,I}}$ in (%/%) of k to reaction $\bar{\sigma}_{x,I}$ as:

$$\bar{S}_{\bar{\sigma}_{x,I}} = \frac{\bar{\sigma}_{x,I}}{k}\frac{\delta k}{\delta\bar{\sigma}_{x,I}} = \frac{-kN_I\{\bar{\phi}^{\dagger}\frac{\partial\bar{\sigma}_{T,I}}{\partial\bar{\sigma}_{x,I}}\bar{\sigma}_x\bar{\phi}\} + kN_I\{\bar{\phi}^{\dagger}\bar{\sigma}_{x,I}\frac{\partial\hat{S}_I}{\partial\bar{\sigma}_x}\bar{\sigma}_{x,I}\bar{\phi}\} + N_I\{\bar{\phi}^{\dagger}\frac{\partial\hat{F}_I}{\partial\bar{\sigma}_{x,I}}\bar{\sigma}_{x,I}\bar{\phi}\}}{\sum_{J\in fissile} N_J\{\bar{\phi}^{\dagger}\hat{F}_J\bar{\phi}\}} \tag{2.7}$$

Once the individual reaction sensitivities are calculated, formula 2.3 may be used to calculate the uncertainty on k_{eff}.
To be able to use equation 2.7 for individual reactions, it is necessary to have access to the cross sections of each reaction. However, as discussed in section 1.3, the multigroup library used by the transport code only contains the lumped scattering matrix $\hat{S}$, cross section σ_{SCAT} and the lumped absorption cross section σ_{ABS}. One can use the lumped reactions in the WIMS library directly (for example [6] perturbs the lumped reactions of the WIMS library and calculates the sensitivities to the lumped cross sections by direct simulations). If this approach is taken, it is difficult to provide valuable feedback to the evaluator regarding the contribution of the reactions (and their energy dependence) to the calculated uncertainty.[3] To overcome this problem, we process each isotope of the JEFF3.1 evaluation with the code NJOY and use the groupr, and wimsr outputs as a database to calculate the reaction sensitivity coefficients defined by equation 2.7. The flowchart presented in the figure 2.1 shows the process of calculating the k_{eff} sensitivity and uncertainty. The sensitivity is calculated according to equation 2.7 in subroutine *susd.py* [4], using the cross sections processed by NJOY. The calculated sensitivity vectors are then used in subroutine *propagate.py* along with a covariance matrix (in NJOY ERRORR format) to estimate the resulting k_{eff} uncertainty according to equation 2.1.

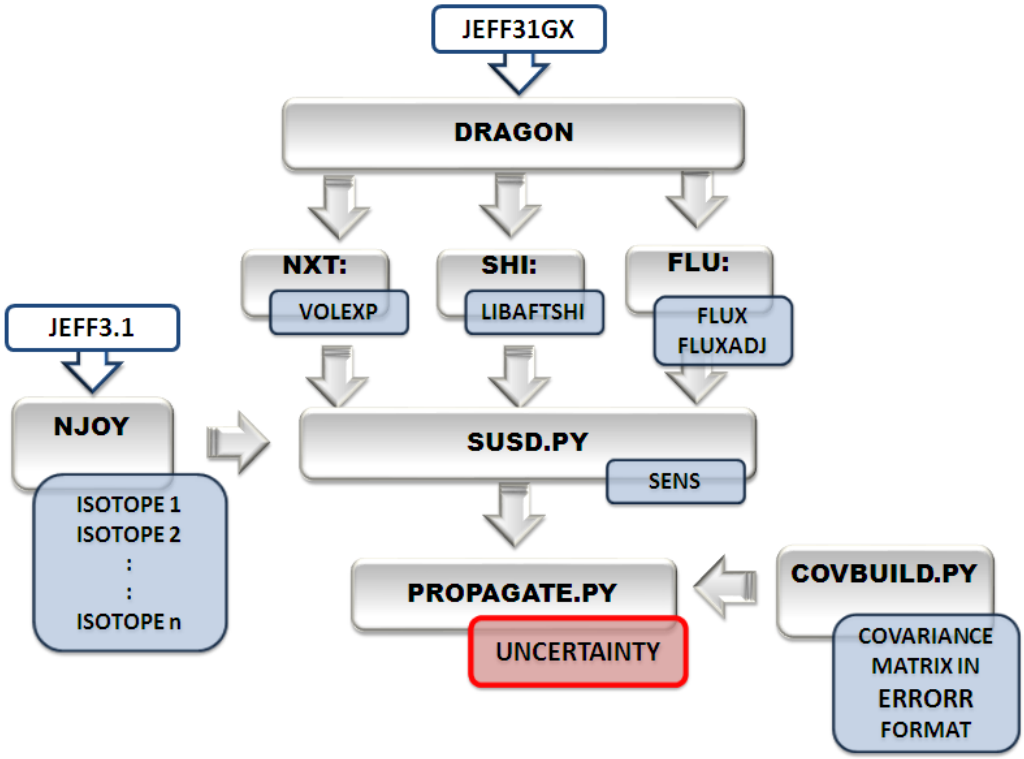

Figure 2.1: Flow chart for Sensitivity and Uncertainty calculations

Table 2.1 presents integrated sensitivities (i.e. $S_{\bar{\sigma}_{x,I}} = \sqrt{\bar{S}_{\bar{\sigma}_{x,I}} \cdot \bar{S}_{\bar{\sigma}_{x,I}}}$), for comparison with those from SCALE6 (ignoring the implicit effect)[23] for ^{238}U and ^{235}U. The presented sensitiv-

[3] Since the measurement techniques and resolutions for the measurement of various scattering and absorption reactions at various energies may be quite different, individual reaction uncertainties are desired.

[4] Note that we have named the subroutine susd due to our previous experience with the code SUSD3D. This is not to say the two codes are in anyway related.

ities are in (%/%), meaning a 1% uniform change in the cross section results in S_x% change in k_{eff}.

Table 2.1: Sensitivities for ^{238}U and ^{235}U

^{235}U

reaction	S_x *susd.py* (%/%)	SCALE (%/%)-EXPLICIT
scattering	-2.72e-4	-1.79 $\cdot 10^{-4}$
capture	-1.52e-1	-1.54e-1
fission	2.52e-1	2.50e-1
nubar	9.34e-1	9.41e-1

^{238}U

reaction	S_x *susd.py* (%/%)	SCALE (%/%)-EXPLICIT
scattering	-9.234e-3	-7.65e-3
fission	3.125e-2	2.857e-2
capture	-2.32e-1	-2.254e-1
nubar	6.06e-2	5.931e-2

The minor differences seen in the scattering sensitivities may result from the basic differences in how the group to group scattering terms are created in the WIMS library and that used by SCALE as well as the number of groups available. Elastic scattering sensitivities for heavy isotopes are generally difficult to compare as the difference formula 2.2 involves the difference of two terms which are roughly equal. The sensitivity for elastic scattering is therefore very dependent on how the outgroup scattering value $S_{g' \to g}$ for $g \neq g'$ is calculated[5]. In the next section we provide a comparison between the uncertainty contributions to k_{eff} predicted by our script *susd.py* using covariance matrices originating from the TALYS data and covariances provided in JENDL-4 and SCALE 6.

2.3 Comparison of the TALYS uncertainties with JENDL-4 and SCALE 6

The function *covbuild.py* was used according to the flowchart shown in figure 2.2 to produce reaction-reaction covariance matrices for ^{235}U and ^{238}U according to equation 2.1. Cross sections originating from each random file were interpolated at 900° K over the self shielding dilution factors outputted by the **SHI:** module of dragon and covariance matrices were produced in NJOY ERRORR format. The python function *propagate.py* was then used to perform the uncertainty propagation using equation 2.1.

[5]In our previous experience with the code SUSD3D, we noticed that this difference is not accurately calculated if single precision is used during the programming

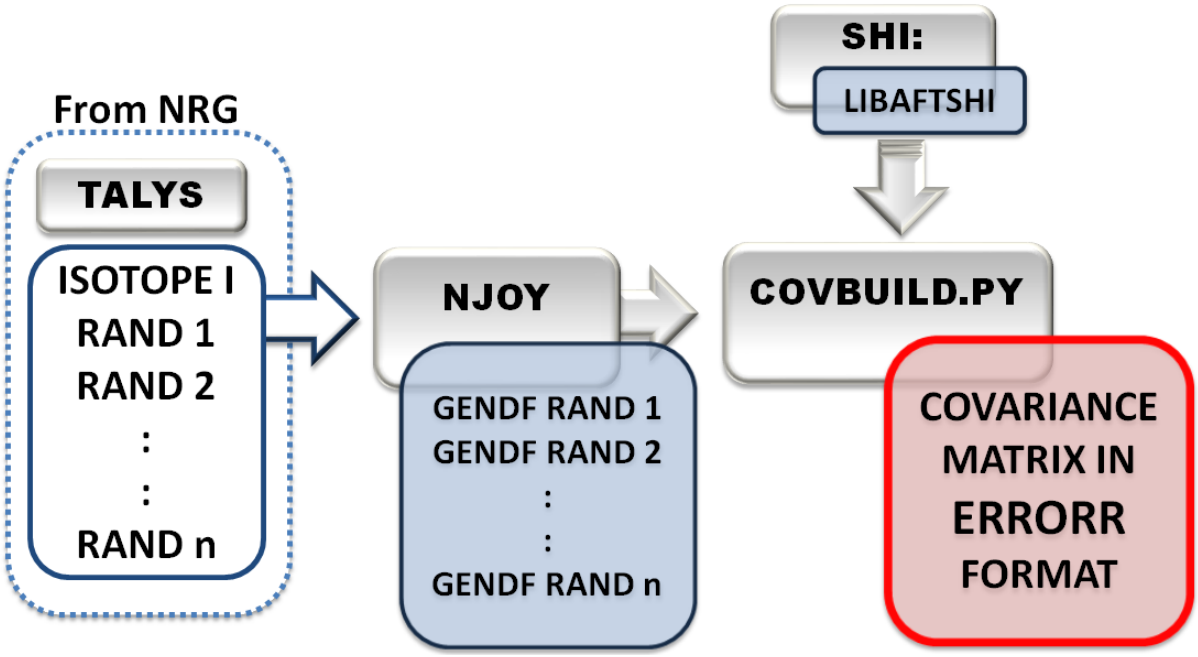

Figure 2.2: Inputs of *covbuild.py*

Figures 2.3 and 2.4 present the resulting distributions of k_{eff} from direct DRAGON simulations using the random multi-group libraries that we have generated according to the flowchart shown in 1.6. For ^{235}U, our estimated uncertainty (0.42%) using classical perturbation theory (with *susd.py*) and the covariance matrices we have built from our random multi-group libraries are in very good agreement with direct simulation results (0.42%). We hope these results present a validation of our methodology in calculating the sensitivity coefficients and for the construction of our covariance matrices. For ^{238}U, the differences are more pronounced. The primary cause of the difference between the uncertainty calculated by *propagate.py* (0.32%) and the uncertainty calculated by direct simulations (0.38%) is our neglect of the implicit effect during the sensitivity calculation in *susd.py*. The implicit effect concerns the sensitivities of the largest heavy nuclide absorber (in this case ^{238}U) and refers to the change in the self shielding mechanism resulting from a change in the cross section. Results from the SCALE code predict a ^{238}U capture sensitivity of $S_{\sigma_{capture}} = -2.15 \times 10^{-1}$ %/% in comparison to our estimated sensitivity of $S_{\sigma_{capture}} = -2.32 \times 10^{-1}$ %/%. Similarily, our scattering sensitivity of $S_{\sigma_{SCAT}} = -9.23 \times 10^{-3}$ %/% is roughly one order of magnitude smaller than that predicted by the SCALE code $S_{\sigma_{SCAT}} = 1.29 \times 10^{-1}$ %/% when the implicit effect is considered. These differences may explain the difference between our predicted uncertainty for ^{238}U and that predicted by direct simulation.

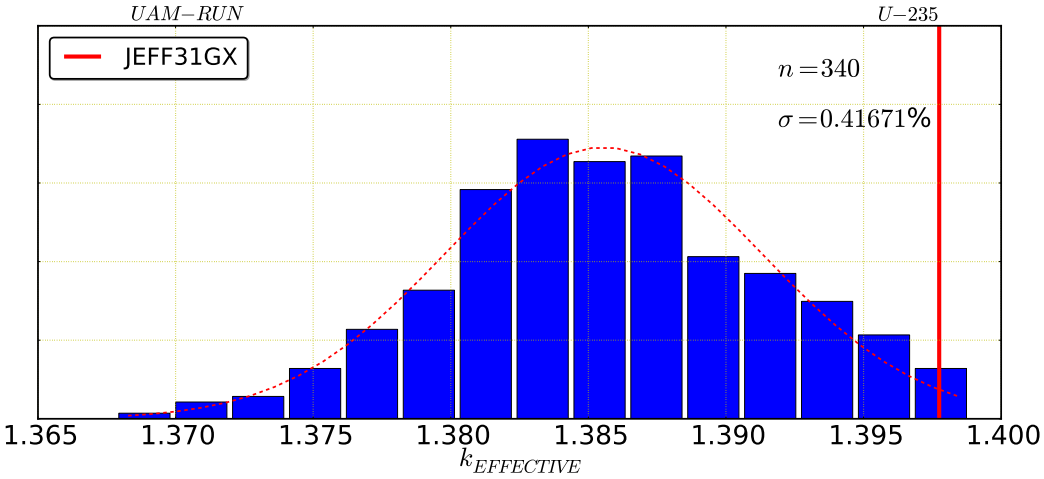

Figure 2.3: Resultant variations of k_{eff} from cross section uncertainties of ^{235}U

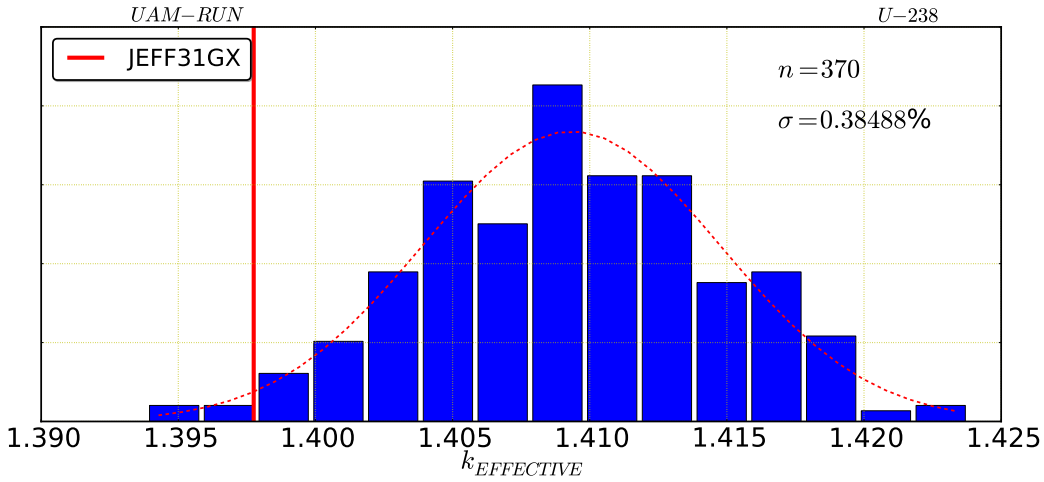

Figure 2.4: Resultant variations of k_{eff} from cross section uncertainties of ^{238}U

Tables 2.2 and 2.3 presents the contribution of the various uncertainties of ^{238} to the k_{eff} uncertainty. The results were obtained by *propagate.py* using the covariance matrices of SCALE (0.38% as shown in 2.3) and the matrices we have built from the TALYS random files (0.42% as shown in 2.2). At a first glance, we can see that the total estimated values of the uncertainties are similar. However, once we compare the contribution of each reaction to the estimated uncertainty, we see that the dominating reaction predicted by the matrices that we have generated is reported to be fission (which contributes to 67.3% of the total uncertainty) while (n, γ) and $\bar{\nu}$ uncertainties are the largest contributers according to the covariances of SCALE.

Table 2.2: Absolute covariance contributions (in **bold**) and percentage contribution (in parenthesis) for ^{235}U from our matrices generated by *covbuild.py* and the TALYS data

U235				**covbuild.py**
REACTION	$(n, n_{elastic})$	(n, f)	(n, γ)	$\bar{\nu}$
$(n, n_{elastic})$	$\mathbf{1.26 \cdot 10^{-12}}$ (0.00)%	$\mathbf{-1.21 \cdot 10^{-9}}$ (-0.01)%	$\mathbf{-8.04 \cdot 10^{-10}}$ (0.00)%	$\mathbf{-6.28 \cdot 10^{-11}}$ (0.00)%
(n, f)	$\mathbf{-1.21 \cdot 10^{-9}}$ (-0.01)%	$\mathbf{1.19 \cdot 10^{-5}}$ (67.30)%	$\mathbf{1.42 \cdot 10^{-6}}$ (7.99) %	$\mathbf{-6.57 \cdot 10^{-7}}$ (-3.71)%
(n, γ)	$\mathbf{-8.04 \cdot 10^{-10}}$ (0.00)%	$\mathbf{1.42 \cdot 10^{-6}}$ (7.99)%	$\mathbf{1.24 \cdot 10^{-6}}$ (6.98)%	$\mathbf{-1.54 \cdot 10^{-7}}$ (-0.87)%
$\bar{\nu}$	$\mathbf{-6.28 \cdot 10^{-11}}$ (0.00)%	$\mathbf{-6.57 \cdot 10^{-7}}$ (-3.71)%	$\mathbf{-1.54 \cdot 10^{-7}}$ (-0.87)%	$\mathbf{3.35 \cdot 10^{-6}}$ (18.90)%
k_{eff} Variance from ^{235}U			$1.771 \cdot 10^{-5}$	
k_{eff} Uncertainty (relative %) from ^{235}U			0.4208 %	

Table 2.3: Absolute covariance contributions (in **bold**) and percentage contribution (in parenthesis) for ^{235}U from the covariance matrices of SCALE-6

U235				**SCALE 6**
REACTION	$(n, n_{elastic})$	(n, f)	(n, γ)	$\bar{\nu}$
$(n, n_{elastic})$	$\mathbf{2.62 \cdot 10^{-14}}$ (0.00)%	$\mathbf{3.92 \cdot 10^{-14}}$ (0.00)%	$\mathbf{-6.08 \cdot 10^{-14}}$ (0.00)%	**0.00** (0.00)%
(n, f)	$\mathbf{3.92 \cdot 10^{-14}}$ (0.00)%	$\mathbf{1.65 \cdot 10^{-6}}$ (11.20)%	**0.00** (0.00) %	**0.00** (0.00)%
(n, γ)	$\mathbf{-6.08 \cdot 10^{-14}}$ (0.00)%	**0.00** (0.00)%	$\mathbf{6.10 \cdot 10^{-6}}$ (41.60)%	$\mathbf{6.93 \cdot 10^{-6}}$ (0.00)%
$\bar{\nu}$	**0.00** (0.00)%	**0.00** (0.00)%	**0.00** (0.00)%	$\mathbf{6.93 \cdot 10^{-6}}$ (47.20)%
k_{eff} Variance from ^{235}U			$1.468 \cdot 10^{-5}$	
k_{eff} Uncertainty (relative %) from ^{235}U			0.3832 %	

Figure 2.5 reports the uncertainty of ^{235}U fission cross section for the three evaluations mentioned. We see that the TALYS output is implicating an uncertainty of approximately 2% on the fission cross section in comparison to the SCALE-6 value of 0.2%. Most likely the uncertainty inputted by the evaluator into TALYS is a bit too large while that of SCALE is underestimated. The JENDL-4 fission uncertainty is highly overestimated in this case and leads to unrealistic results (k_{eff} uncertainty of 1.2%). We have therefore not provided JENDL-4 comparisons for ^{235}U.

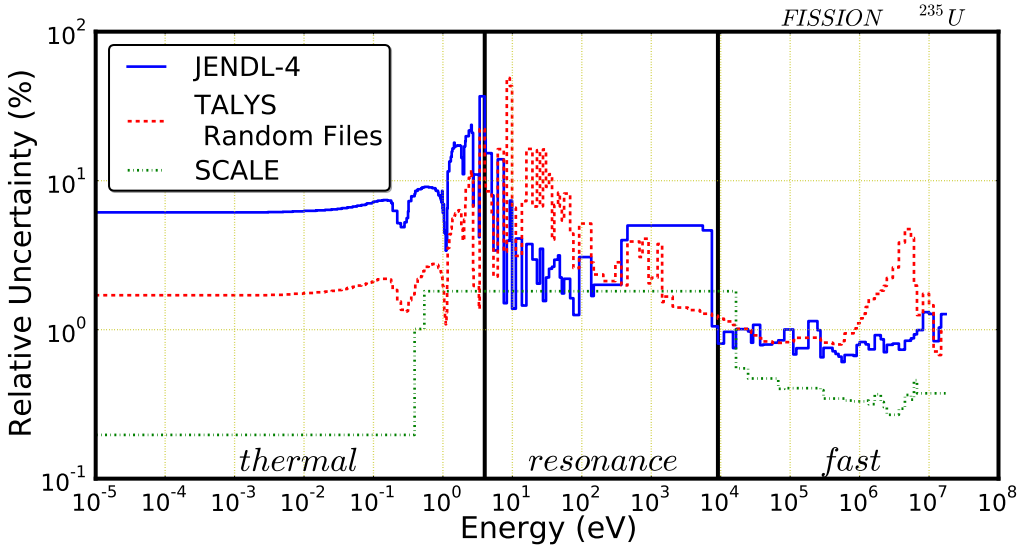

Figure 2.5: Comparison of the fission cross section uncertainty between the TALYS generated covariances, SCALE-6, and JENDL-4 covariances

Table 2.4, 2.5, and 2.6 show the contributions of the reactions of ^{238}U to the k_{eff} uncertainty predicted by our generated covariances from TALYS, and those of JENDL-4 and SCALE-6 using *propagate.py*.

Table 2.4: Absolute covariance contributions (in **bold**) and percentage contribution (in parenthesis) for ^{238}U from our matrices generated by *covbuild.py* and the TALYS data

U238				**covbuild.py**
REACTION	$(n, n_{elastic})$	(n, f)	(n, γ)	$\bar{\nu}$
$(n, n_{elastic})$	$\mathbf{5.37 \cdot 10^{-8}}$ (0.535)%	$\mathbf{-2.87 \cdot 10^{-9}}$ (-0.0286)%	$\mathbf{3.90 \cdot 10^{-7}}$ (3.89)%	$\mathbf{-2.94 \cdot 10^{-8}}$ (-0.293)%
(n, f)	$\mathbf{-2.87 \cdot 10^{-9}}$ (-0.0286)%	$\mathbf{2.39 \cdot 10^{-7}}$ (2.38)%	$\mathbf{5.67 \cdot 10^{-9}}$ (0.0565)%	$\mathbf{-1.39 \cdot 10^{-7}}$ (-1.39)%
(n, γ)	$\mathbf{3.90 \cdot 10^{-7}}$ (3.89)%	$\mathbf{5.67 \cdot 10^{-9}}$ (0.0565)%	$\mathbf{4.98 \cdot 10^{-6}}$ (49.6)%	$\mathbf{3.92 \cdot 10^{-8}}$ (0.391)%
$\bar{\nu}$	$\mathbf{-2.94 \cdot 10^{-8}}$ (-0.293)%	$\mathbf{-1.39 \cdot 10^{-7}}$ (-1.39)%	$\mathbf{3.92 \cdot 10^{-8}}$ (0.391)%	$\mathbf{4.11 \cdot 10^{-6}}$ (41)%
k_{eff} Variance from ^{238}U			$1.003 \cdot 10^{-3}$ %	
k_{eff} Uncertainty (relative %) from ^{238}U			0.3168 %	

Table 2.5: Absolute covariance contributions (in **bold**) and percentage contribution (in parenthesis) for ^{238}U from the covariance matrices of JENDL-4

U238				**JENDL − 4**
REACTION	$(n, n_{elastic})$	(n, f)	(n, γ)	$\bar{\nu}$
$(n, n_{elastic})$	$\mathbf{3.16 \cdot 10^{-10}}$ (0.00%)	$\mathbf{-6.55 \cdot 10^{-13}}$ (-0.00%)	$\mathbf{4.48 \cdot 10^{-9}}$ (0.04%)	**0.00** (0.00%)
(n, f)	$\mathbf{-6.55 \cdot 10^{-13}}$ (0.00%)	$\mathbf{3.26 \cdot 10^{-8}}$ (0.28%)	$\mathbf{5.57 \cdot 10^{-11}}$ (0,00%)	**0.00** (0.00%)
(n, γ)	$\mathbf{4.48 \cdot 10^{-9}}$ (0,04%)	$\mathbf{5.57 \cdot 10^{-11}}$ (0.00%)	$\mathbf{1.07 \cdot 10^{-5}}$ (91.40%)	**0** (0.00 %)
$\bar{\nu}$	**0.00** (0.00%)	**0.00** (0.00%)	**0.00** (0.00%)	$\mathbf{1.45 \cdot 10^{-7}}$ (1.24%)
k_{eff} Variance from ^{238}U			$1.171 \cdot 10^{-3}$ %	
k_{eff} Uncertainty (relative %) from ^{238}U			0.3422 %	

Table 2.6: Absolute covariance contributions (in **bold**) and percentage contribution (in parenthesis) for ^{238}U from the covariance matrices of SCALE 6

U238				**SCALE**
REACTION	$(n, n_{elastic})$	(n, f)	(n, γ)	$\bar{\nu}$
$(n, n_{elastic})$	$\mathbf{5.33 \cdot 10^{-9}}$ (0,04%)	$\mathbf{-3.58 \cdot 10^{-12}}$ (-0.00%)	$\mathbf{1.93 \cdot 10^{-7}}$ (1.43%)	**0** (0.00%)
(n, f)	$\mathbf{-3.58 \cdot 10^{-12}}$ (-0.00%)	$\mathbf{8.64 \cdot 10^{-8}}$ (0.64%)	$\mathbf{-3.33 \cdot 10^{-10}}$ (-0.00%)	**0.00** (0.00%)
(n, γ)	**1.93E − 07** (1.43%)	$\mathbf{-3.33 \cdot 10^{-10}}$ (-0.00%)	$\mathbf{1.29 \cdot 10^{-5}}$ (95.4%)	**0.00** (0.00%)
$\bar{\nu}$	**0** (0.00%)	**0** (0.00%)	**0.00** (0.00%)	$\mathbf{1.52 \cdot 10^{-7}}$ (1.12%)
k_{eff} Variance from ^{238}U			$1.356 \cdot 10^{-3}$ %	
k_{eff} Uncertainty (relative %) from ^{238}U			0.3682 %	

Once again, the predicted total uncertainty is similar for the three libraries but the contributions are quite different. Particularly, we see our second dominating term that is coming from our covariances is the $\bar{\nu}$ uncertainty of ^{238}U (accounting for 41% of the k_{eff} uncertainty). This is when only 6% of the fission contribution is due to ^{238}U fission. Presented in figure 2.6 are the $\bar{\nu}$ uncertainties reported by each library. We see that in the fast range, the $\bar{\nu}$ uncertainty we have generated from the TALYS random files is roughly one order of magnitude higher than that of the other two libraries. The evaluator[6] acknowledges that the $\bar{\nu}$ uncertainty is overestimated and the correct uncertainty (1%) will be used in the next evaluation.

[6]Private correspondence with Dr. D. Rochman at NRG

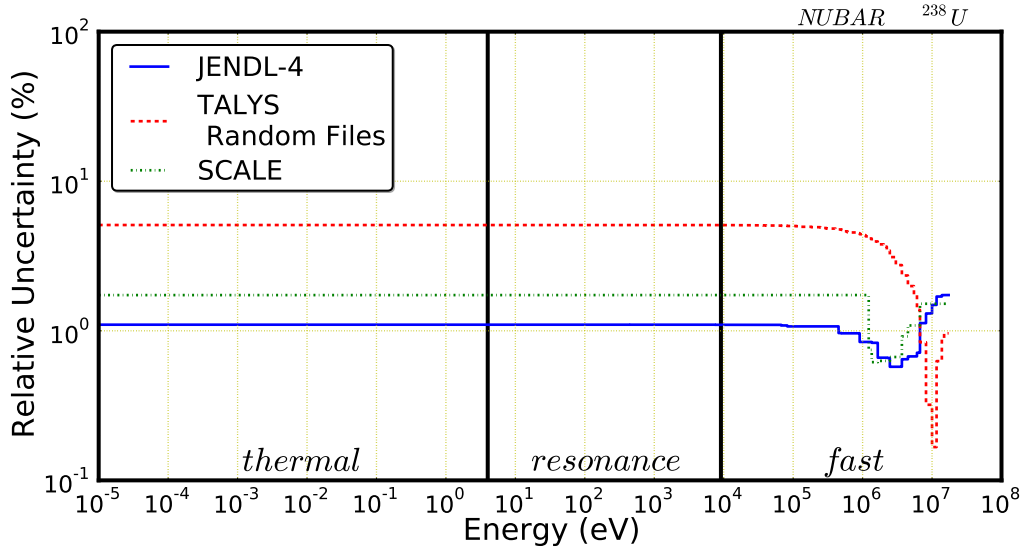

Figure 2.6: Comparison of the ^{238}U $\bar{\nu}$ uncertainty between the TALYS generated covariances, SCALE-6, and JENDL-4 covariances

Appendix A provides comparisons between the three libraries for the other major reactions. We note at this point that as the idea of providing covariance matrices is a new one, the data is still in its infancy. Presently, most of the covariances provided by evaluators are a mix of experimental uncertainties and evaluation uncertainties (if available) and intelligent guesses of the form of the covariances between the various data. Sometimes, the provided matrices are not positive definite (for example, [6] has encountered negative eigenvalues for some of the SCALE 6 matrices). Provided that cross section parameter covariances are provided by the evaluator, propagation and presentation in multi-group format is not a simple process (particularly because of self shielding). The benefit of our approach with the data of NRG is that we construct covariances which in the ideal are results of a proper propagation of errors through the evaluation process. Additionally, since we calculate the covariances from the random samples of the multi-group libraries, they are guaranteed to satisfy the conditions of covariance matrices 2.3. Given the large amount of data available in the library, propagation through self shielding calculation reduces to simply interpolation of the data at the desired parameters (temperature and dilution) and constructing the covariances between the interpolated parameters.

Chapter 3

Burnup

In evolution calculations one is concerned with the long term fuel composition change over the fuel life cycle. In order to have a profile of the various reactor parameters (k_{eff}, fission rates, fluxes, and etc.) one is obligated to track the fuel composition throughout the course of the cycle. Since the effect is coming from isotopic density changes in the fuel due to irradiation by the neutron flux and mutation (through nuclear decay) of the resulting child nuclei, the fuel isotopic density variation may be considered slow. Therefore, what is done by most codes [24] is to split the problem into two parts; at each time step a static flux solution of the steady state Boltzmann equation (ignoring the flux time derivative) is calculated. The Batemann equations are then solved with the calculated flux giving the updated isotopic densities/composition to be used for the next time step.

3.1 Definitions

In our previous work with MURE [7], due to the statistical nature of the solution, we had seen two sources of errors-those originating from uncertainties inherent in nuclear data as well as the statistical error originating from the stochastic nature of the solution. Although the goal of the investigation was to study the uncertainty on isotopic density changes, the statistical error for some of the isotopes (eg. ^{237}Np, ^{241}Pu) was the dominating factor which rendered analysis of such isotopes impossible.
Contrary to our previous approach, a deterministic approach provides a fast[1] and fairly accurate [25] method for evolution calculations with no statistical errors. The trade off is the additional effort that must be put into the process of library production as described in Chapter 1. In this chapter, we present results to the UAM Benchmark I.b [19] using the collective set of TALYS generated random libraries that we have processed.

3.1.1 Isotopic Densities

As shown in figure 3.3, the process of burnup involves the creation and decay of a number of isotopes. For Uranium Oxide fuels involving various enrichments of ^{235}U, the isotopes initially present in the fuel are ^{238}U and ^{235}U.

For isotopes I at time t that are initially present in the fuel, we define the uncertainty of the isotopic density $\sigma(N_I^t)$ and the uncertainty of the isotopic density **change** $\sigma(\Delta N_I^t)$ relative to

[1] for example we ran 6 simulations in 1 hour of simulation on the LPSC server

the initial density present in the fuel as:

$$(\sigma(N_I^t))^2 = \frac{\mathbb{E}[(N_I^t)^2]}{(N_I^0)^2} \tag{3.1}$$

$$(\sigma(\Delta N_I^t))^2 = \frac{\mathbb{E}[(N_I^t - \bar{N}_I^t)^2]}{(\bar{N}_I^t - N_I^0)^2} \tag{3.2}$$

For isotopes which are not present at the start of the fuel cycle such as ^{239}Pu, ^{238}Pu, ^{237,239}Np, ..., we define the absolute uncertainty of the isotopic change at time $t > 0$ as:

$$\sigma_{\Delta N_I}^t = \frac{\mathbb{E}[(N_I^t - \bar{N}_I^t)^2]}{(\bar{N}_I^t)^2} \tag{3.3}$$

3.1.2 Flux Uncertainties

The cell power $P(t)$ at time t may be defined as:

$$P(t) = \sum_{I \in fissile} N_I^t \sum_g \vec{\sigma}_{I,fission} \cdot \vec{\phi}^t E_f^I \tag{3.4}$$

where $\vec{\phi}_t = (\phi^t)_{g,v} \in \mathbb{R}^{V \times G}$ is the flux spectrum at time t, $\sigma_{I,fission} = (\sigma_{I,fission})_{g,v}$ is the fission cross section for isotope I at group $g \in \{1, .., G\}$ and volume $v \in fuel$, E_f^I is the average energy released per fission of isotope I, and the operator $(\cdot)$ represents integration over energy and space.
As the benchmark[19] requested calculations to be performed at the constant power of $P(t)$= 25 $\frac{KW}{KgU}$, the left side of 3.4 is held constant. Therefore, with the evolution of the isotopic densities N_I^t as a function of time one may expect a resultant shift in the flux spectrum. Furthermore, since the isotopic densities are directly related to reaction rates (production - loss), the temporal behavior of the isotopic densities, as well as their corresponding uncertainties, are found to have a correspondence with the flux $\phi = (\phi)_g$ and its uncertainty.
Figure 3.1 presents the isotopic fission contributions (in % of the total fission rate) for ^{235}U, ^{238}U, and ^{239}Pu as a function of burnup $\frac{\text{MWd}}{\text{kg}}$. One sees the shift in the fission contribution[2] from that of ^{235}U to ^{239}Pu resulting from the burnup of ^{235}U and the production of ^{239}Pu. The accompanying figure shows the hardening of the flux spectrum as a function of time due to the accumulation of Pu isotopes. Particularly, the buildup of ^{240}Pu with its large resonance ($\sim 10^5$ barns) at $\sim 1eV$ results in a reduction of the flux at thermal energies and a hardening of the flux (note the increase in ^{238}U fast fission contribution).

[2]Considered contribution from ^{235}U,^{238}U,$^{239-242}$Pu

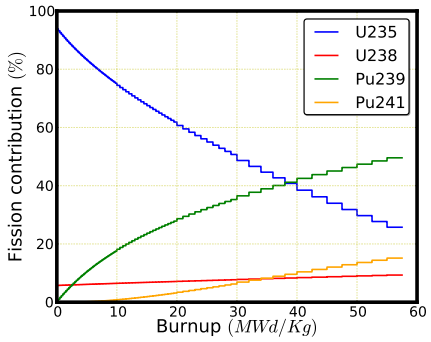

Figure 3.1: Isotopic fission contribution with time

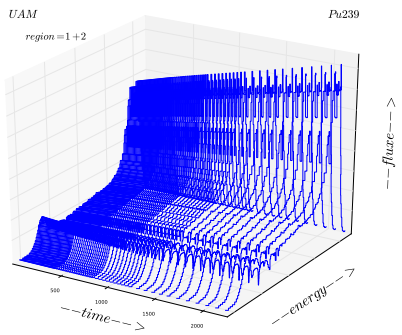

Figure 3.2: Example of flux evolution due to Plutonium buildup

To simplify the analysis that follows, we define the one group condensed cross sections $\sigma^t_{I,x}$ for reaction x of isotope I at time t as:

$$\sigma^t_{I,x} = \frac{\vec{\sigma}_{I,x} \cdot \vec{\phi}^t}{\vec{\phi}^t \cdot \vec{1}} = \frac{\vec{\sigma}_{I,x} \cdot \vec{\phi}^t}{\phi^t} \tag{3.5}$$

where $\vec{1}$ represents the vector containing ones in its entries and $\phi^t = \vec{\phi}^t \cdot \vec{1}$. The reaction rate $R^t_{I,x}$ may then be defined as:

$$R^t_{I,x} = N_I \vec{\sigma}_{I,x} \cdot \vec{\phi}^t = N_I \sigma^t_{I,x} \phi^t \tag{3.6}$$

3.1.3 Isotopic Mass Changes

The evolution of the isotopic density for an isotope is governed by the difference between the factors that result in the production of the isotope and those that result in the loss of the isotope. For an isotope I, the isotopic density **change** $\Delta N^{t_n}_I$ at time t can be written described by:

$$\begin{aligned} \Delta N^t_I &= -\sum_{J \neq I} \int_0^t N^t_I \lambda_{I \to J} dt - \sum_x \int_0^t N^t_I \sigma^t_{I,x} \phi^t dt + \sum_{J, J \neq I}^{M} \sum_y \int_0^t N^t_J \sigma^t_{J,y_I} \phi^t dt \\ &+ \sum_{J, J \neq I}^{M} \int_0^t N^t_J \lambda_{J \to I} dt \end{aligned} \tag{3.7}$$

where $\lambda_I = \frac{ln(2)}{T^I_{1/2}}$ represents the decay life constant of isotope I, x represents reactions which result in the loss of isotope I (mainly through capture and fission), y_I represents reactions of isotope J which result in creation of isotope I, and $\lambda_{J \to I}$ represents the decay life constant of isotope J to isotope I. We note if the half life $T^L_{1/2}$ is much larger than the time step, we may ignore the the first term (for $I = L$) or the last term (for $J = L$) without any complications.

Figure 3.3 presents a simplified version of the possible decay chains for the isotopes considered in this work.

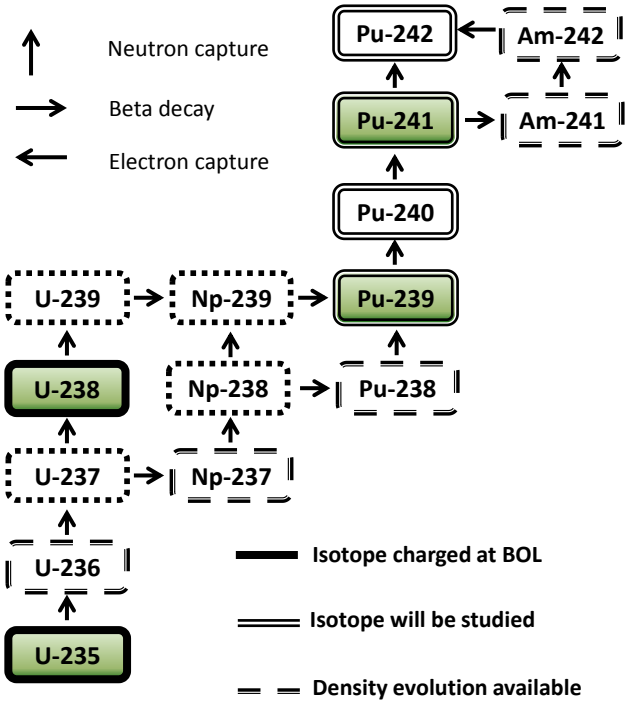

Figure 3.3: Production and decay for the most important isotopes in the UAM Benchmark

3.2 Uncertainties of ^{235}U Density

Since ^{235}U is present at the start of the cycle, we define the uncertainties associated with the isotopic density $\sigma(N_I^t)$ and isotopic density change $\sigma(\Delta N_I^t)$ according to equation 3.1. We note that for ^{235}U, the only term present in equation 3.7 is loss due to capture and fission. Therefore, equation 3.7 simplifies to:

$$N_{235U}^t = -\int_0^t N_{235U}^0 \phi^t \{\sigma_{235U,f}^t + \sigma_{235U,(n,\gamma)\rightarrow^{236}\mathrm{U}}^t\} dt \tag{3.8}$$

Figures 3.4 show the spread in the ^{235}U density as a function of time (in days) due to uncertainties in the cross sections of ^{235}U, ^{238}U, ^{239}Pu, and ^{241}Pu. As a result of burnup, we note that at the end of the cycle, the density of ^{235}U is reduced to approximately 85% of the initial density N_{235U}^0. This explains the shift in the fission contribution from that of ^{235}U to ^{239}Pu observed in figure 3.1 of the previous section.

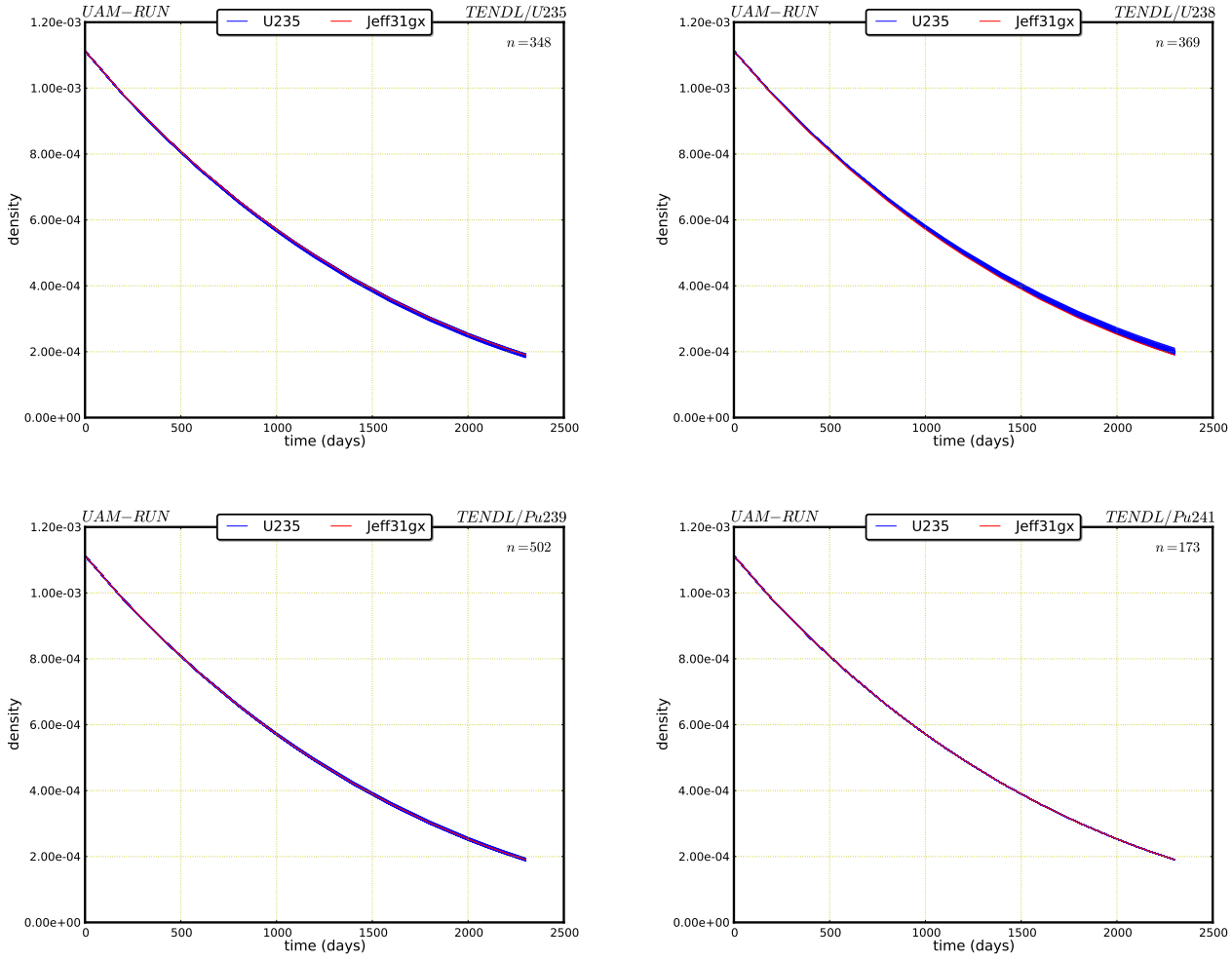

Figure 3.4: U^{235} density evolution due to cross section uncertainties of U^{235},U^{238},Pu^{239} and Pu^{241}

3.2.1 Uncertainties due to variations in the cross sections of ^{235}U

From differentiation of 3.8 with respect to time, we note that the density of ^{235}U satisfies:

$$\frac{\partial N^{U235}}{\partial t} = -\left(\sigma_c + \sigma_f\right) \cdot \phi \cdot N \tag{3.9}$$

We can therefore express the density change ΔN^{U235} as a function of time:

$$\Delta N^{U235} = \int_0^t \frac{\partial N^{U235}}{\partial t} = -\int_0^t \left(\sigma_c + \sigma_f\right) \cdot \phi \cdot N \cdot dt \tag{3.10}$$

Defining the sensitivity coefficient (in $\%/\%$) of ΔU^{235} with respect to the parameter $\alpha \in \{\sigma_c + \sigma_f, \phi, N\}$ as:

$$S_\alpha = \frac{\alpha}{\Delta N^{U235}} \cdot \frac{\partial \Delta N^{U235}}{\partial \alpha} \tag{3.11}$$

we have:

$$S_\phi = \frac{\phi}{\Delta N^{U235}} \cdot \frac{\partial \Delta N^{U235}}{\partial \phi} = \frac{\left(-\int_0^t \left(\sigma_c + \sigma_f\right) \cdot N^{U235} \cdot dt\right) \cdot \phi}{-\int_0^t \left(\sigma_c + \sigma_f\right) \cdot N^{U235} \cdot \phi \cdot dt} = 1.0 \tag{3.12}$$

$$S_{N^{235U}} = \frac{N^{U235}}{\Delta N^{U235}} \cdot \frac{\partial \Delta N^{U235}}{\partial N^{U235}} = \frac{\left(-\int_0^t (\sigma_c + \sigma_f) \cdot \phi \cdot dt\right) \cdot N^{U235}}{-\int_0^t (\sigma_c + \sigma_f) \cdot N^{U235} \cdot \phi \cdot dt} = 1.0 \tag{3.13}$$

and

$$S_{\sigma_c+\sigma_f} = \frac{(\sigma_c + \sigma_f)}{\Delta N^{U235}} \cdot \frac{\partial \Delta N^{U235}}{\partial (\sigma_c + \sigma_f)} = \frac{\left(-\int_0^t N^{U235} \cdot \phi \cdot dt\right) \cdot (\sigma_c + \sigma_f)}{-\int_0^t (\sigma_c + \sigma_f) \cdot N^{U235} \cdot \phi \cdot dt} = 1.0 \tag{3.14}$$

Using the law of propagation of errors described by equation 2.3, we can calculate the error of the first time step by:

$$\begin{aligned} \sigma\left(\Delta N\right)^2 &= \left((\phi \cdot \Sigma_a)^2 \cdot \sigma(N)^2 + (N \cdot \Sigma_a)^2 \cdot \sigma(\phi)^2\right. \\ &+ \left.(N \cdot \phi)^2 \cdot \sigma(\Sigma_a)^2 + 2 \cdot N^2 \cdot \Sigma \phi cov\left(\phi, \Sigma_a\right)\right) \cdot \Delta t \end{aligned} \tag{3.15}$$

so that:

$$\frac{\sigma\left(\Delta N\right)^2}{\Delta N^2} = \left(\frac{\sigma(\phi)^2}{\phi^2} + \frac{\sigma(\Sigma)^2}{\Sigma^2} + 2 \cdot \frac{cov\left(\phi, \Sigma_a\right)}{\phi \Sigma}\right) \cdot \tag{3.16}$$

For the first time step, the values of the above equation are : $\left(\frac{\sigma(\phi)}{\phi} = 0.5162\%\right)$, $\left(\frac{\sigma(\Sigma)}{\Sigma} = 0.32609\%\right)$ and the contribution from the covariance between ϕ and Σ $2 * \frac{cov(\phi,\Sigma_a)}{\phi^2\Sigma^2} = -28.735\%$ resulting in a mass density error of $\frac{\sigma(\Delta N)}{\Delta N} = 0.346\%$.

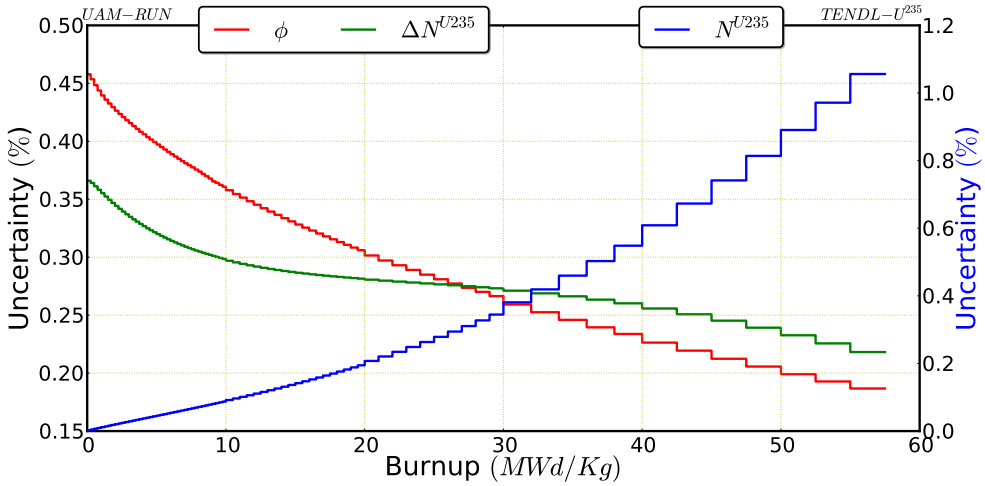

Figure 3.5: Evolution of the flux ϕ, density N^{235} and density change ΔN^{235} due to uncertainties of ^{235}U

3.2.2 Uncertainties due to variations in the cross sections of ^{238}U

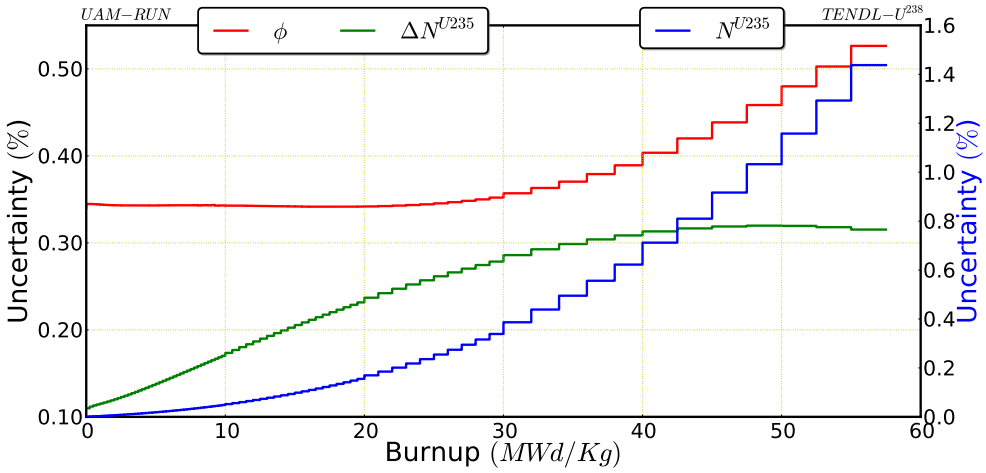

Figure 3.6: Uncertainty evolution as a result of the uncertainties of ^{238}U

Appendix A shows the uncertainty on the fission cross section of ^{238}U to be $\sim$ 6% at high energies. Given that the fission rate is constant (see figure 3.1) at the start of the cycle, and slightly augments with the hardening of the spectrum, one can expect the resultant uncertainty on the flux due to the fission of ^{238}U to approximately be:

$$\sigma(\phi) = \sigma(\sigma_{238U,f}) * \frac{\text{fission rate of } ^{238}U}{\text{total fission rate}} \tag{3.17}$$

As figure 3.1 shows, approximately 6% of the fission rate comes from ^{238}U with the uncertainty of approximately 5% after the thresh hold boundary. One would therefore expect an uncertainty on the flux of approximately 0.3% with a trend of gradual increase corresponding with the gradual increase in the fission contribution of ^{238}U.
With the buildup of ^{239}Pu and its progenies (particularly ^{240}Pu), and noting that the uncertainties in the capture of ^{238}U will naturally affect the concentration of ^{239}Pu, the correlations between the flux and ^{238}U increases. Therefore one can expect an increasing trend in the flux uncertainty coming from the correlation of the flux with ^{238}U through ^{239}Pu. Figure 3.1 presents the resultant uncertainty in the ^{235}U density orignating from cross section uncertainties of ^{238}U.

3.2.3 Uncertainties due to variations in the cross sections of ^{239}Pu

Figure 3.7 presents the uncertainty variation of the atomic density and the density change of ^{235}U originating from the cross section uncertainties of ^{239}Pu. At the start of life, there is almost no effect coming from the ^{239}Pu to the flux (due to fission) and its spectrum (resonances of its progenies such as ^{240}Pu at 1 eV). The gradual increase in the flux uncertainty results from the incrementing correlation between the flux and ^{239}Pu as its concentration increases. The effect of ^{239}Pu on the flux is contribution to fission and a hardening of the flux spectrum which results from the build up of ^{239}Pu and the subsequent creation ^{240}Pu from its parent ^{239}Pu. As the concentration of ^{239}Pu, ^{240}Pu increases due to capture reactions of ^{238}U, the flux shifts to a more rapid spectrum. The result is a gradual increase in ^{235}U one group average cross section

uncertainties(in particular the fission cross section uncertainty) resulting from a the flux and flux spectrum uncertainties. (these can be uncertainty in the self shielding i.e. the capture resonance of ^{241}Pu 1eV of 10^5 barns results in the reduction of the thermal flux).

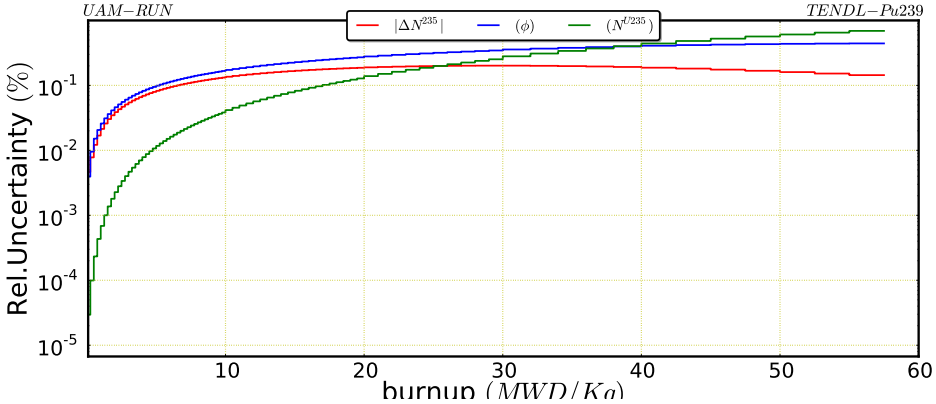

Figure 3.7: Uncertainty evolution as a result of the uncertainties of ^{239}Pu

3.3 Uncertainties of ^{238}U Density

We observe from the decay chain for ^{238}U presented in figure 3.3, that at the start of life there are no neighboring nuclei from which ^{238}U may be produced. Therefore, the only effect on the ^{238}U density is that due to loss by capture/fission reactions. Equation 3.18 presents a simplified representation of the density change of ^{238}U as a function of time.

$$\Delta N^{U238}(t) = \int_0^t N^{U238}(t) \cdot \phi^g(t) \ \cdot \sigma_f^g(t) \cdot dt - \int_0^t N^{U238}(t) \cdot \phi^g(t) \cdot \sigma_c^g(t) \cdot dt \tag{3.18}$$

From figures 3.8 one can see that the ^{238}U density is slow over the long course of the burnup. The largest contribution to the error is that coming from the reactions of ^{238}U (i.e $N^{238}, N^{238} \cdot \Sigma_f^{238}, N^{238} \cdot \Sigma_{c\to^{239}U}^{238}, ...$). We can therefore expect little contribution from other nuclei uncertainties which only affect the ^{238}U density changes through feedback by the flux level.

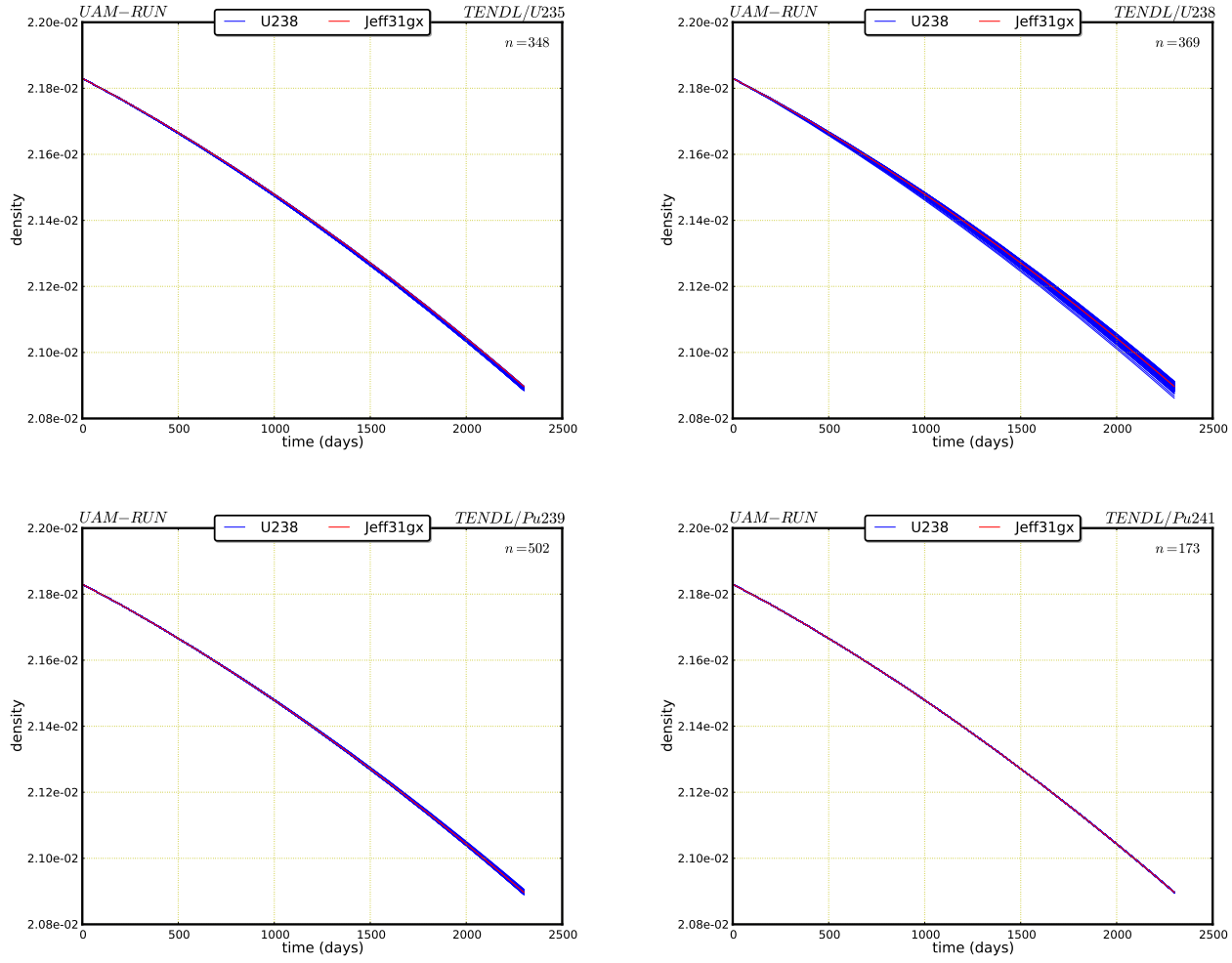

Figure 3.8: U^{238} density by cross section changes in U^{235},U^{238},Pu^{239} and Pu^{241}

3.3.1 Uncertainties due to variations in the cross sections of ^{235}U

For ^{238}U at the start of life, the only contributing factor due to the uncertainties of ^{235}U is the correlation with the flux. The main reaction of ^{235}U which affects the flux is fission. Uncertainties in the ^{235}U fission will affect the magnitude of the fission source and therefore the flux amplitude/level. Therefore, the main source of the uncertainty is expected to come from the flux level feedback originating from the cross section uncertainties of ^{235}U. This explains the well correspondence between the uncertainty of ΔN_{238} and the flux uncertainty (i.e. the two are reported as the same at 0.45%).
Unfortunately, at this point, we do not understand the behavior of the ΔN_{238} uncertainty in the few hundred days. The global decreasing trend with of the uncertainty (both on the flux, and density changes of ^{238} U), is due to the diminishing effect/role of ^{235}U in the core which results as a result of the build up of ^{239}Pu and its increasing contribution to fission.

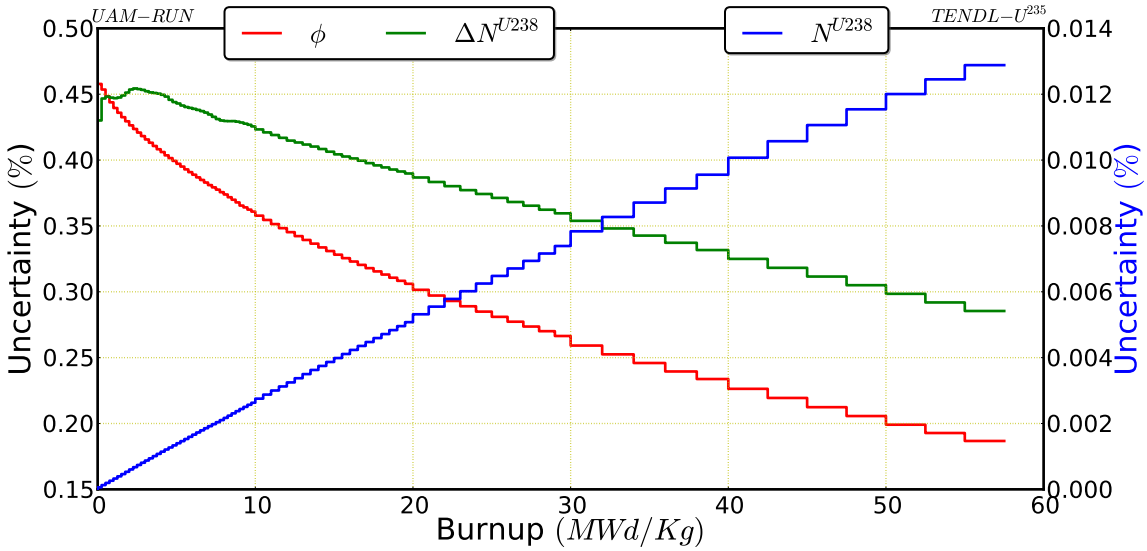

Figure 3.9: Uncertainty evolution as a result of the uncertainties of ^{235}U

3.3.2 Uncertainties due to variations in the cross sections of ^{238}U

As discussed earlier, the main contribution to the ^{238}U would be that of its own cross section uncertainties, and in comparison, a smaller contribution from the flux feedback. Figure 3.10 presents the uncertainty of the density and density change of ^{238}U as a function of burnup.

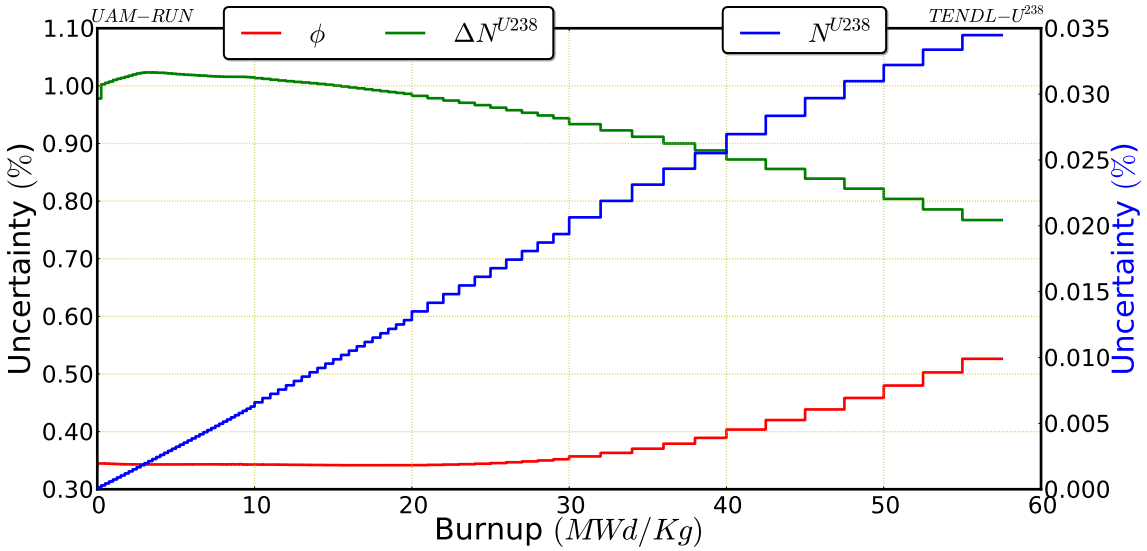

Figure 3.10: Uncertainty evolution as a result of the uncertainties of ^{238}U

Given that the capture uncertainty (see chapter 2) of ^{238}U within the thermal range is about 0.58% and within resonance range is roughly about 2%, we can expect an uncertainty on the density change of ^{238}U (and its children at the start of the cycle) to be of the same order (explaining the 1% uncertainty observed in figure 3.10). With the gradual build of the progenies

of ^{238}U, the dependence/correlations between the flux and its spectrum with ^{238}U increases through their correlations with ^{239}Pu.

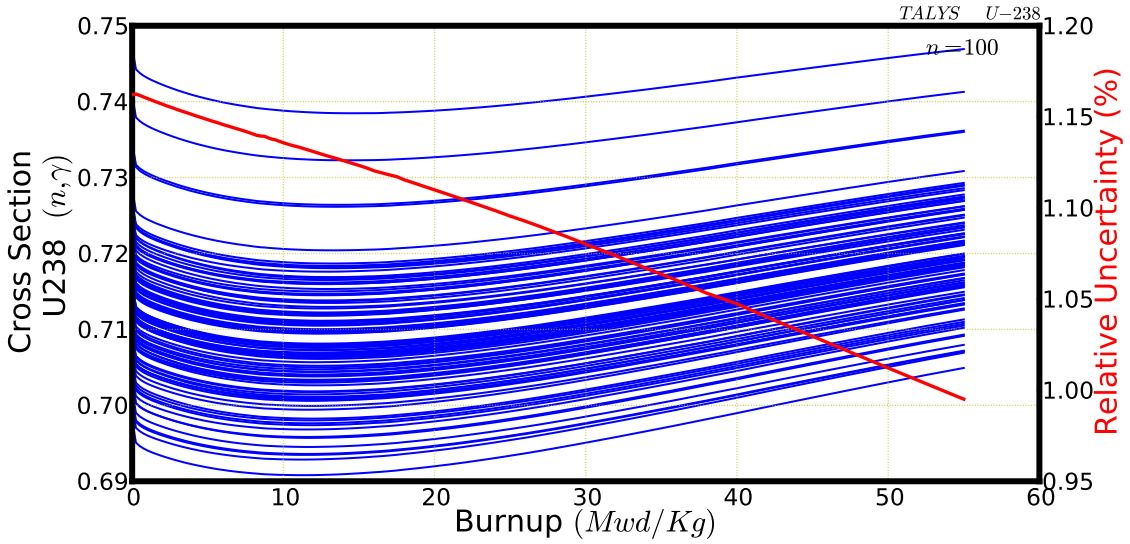

Figure 3.11: ^{238}U capture cross section over the time

3.4 Uncertainties of ^{239}Pu

Important reactions for the production and loss of ^{239}Pu are production by means of ^{238}U radiative capture (equation 3.19) and loss by ^{239}Pu fission and radiative capture (resulting in the production of ^{240}Pu). Figure 3.12 shows the evolution with time of the ^{239}Pu density as well as the spread that results due to uncertainties inherent in cross section data of ^{235}U, ^{238}U, ^{239}Pu and ^{241}Pu. We note that at the end of the cycle, there is a rough equilibrium between the production of ^{239}Pu by (n,γ) of ^{238}U and loss of ^{239}Pu from fission and radiative capture reactions. The trend can be observed in the figure below with the convergence to a constant asymptote. Equation 3.20 presents a simplified form of the evolution of the change in the 239Pu density as a function of time. Therefore, one is to expect that the nuclei (i.e. ^{238}U, ^{239}Pu) which appear directly in equation 3.20 will have a major effect on the uncertainty. Variations of other nuclei (such as ^{235}U, ^{241}Pu) can affect the ^{239}Pu density only through feedback effects which result from uncertainties in the flux and its spectrum.

$$U^{238} \xrightarrow{n,\gamma} U^{239} \xrightarrow{\beta^-} Np^{239} \xrightarrow{\beta^-} Pu^{239} \tag{3.19}$$

Since the half life $T_{1/2}$ for U^{239} and Np^{239} are 23 min and 2 days we may write:

$$\Delta N^{239} = N^{239}(t) = \underbrace{\int_o^t N^{238} \cdot \phi \cdot + \Sigma_c^{238} \cdot dt}_{\text{Production}} - \underbrace{\int_o^t N^{239} \cdot \phi \cdot \left(\Sigma_f^{239} + \Sigma_c^{239}\right) \cdot dt}_{Consumption} \tag{3.20}$$

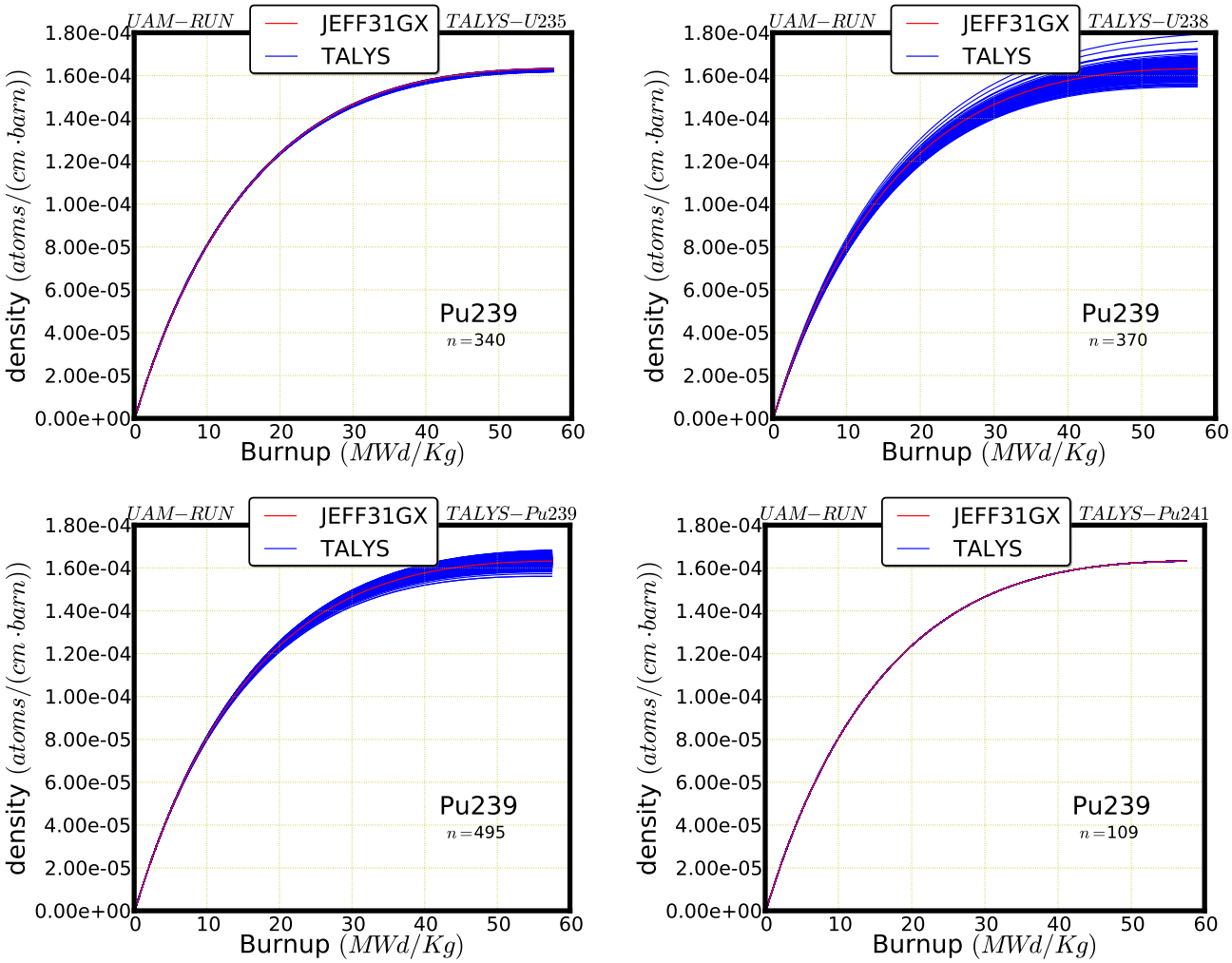

Figure 3.12: Pu^{239} density evolution due to cross section variations in U^{235},U^{238},Pu^{239} and Pu^{241}

3.4.1 Uncertainties due to variations in the cross sections of ^{238}U

As described earlier in section 3.1.3, at the start of cycle the only contribution to the uncertainty of the density change of ^{239}Pu can come from the uncertainties present in the capture of ^{238}U. Figure 3.13 shows the negative correlations (-0.8831) between ^{238}U densities and ^{239}Pu densities. One can see that the extra losses of ^{238}U translate to an increase in the production of ^{239}Pu.

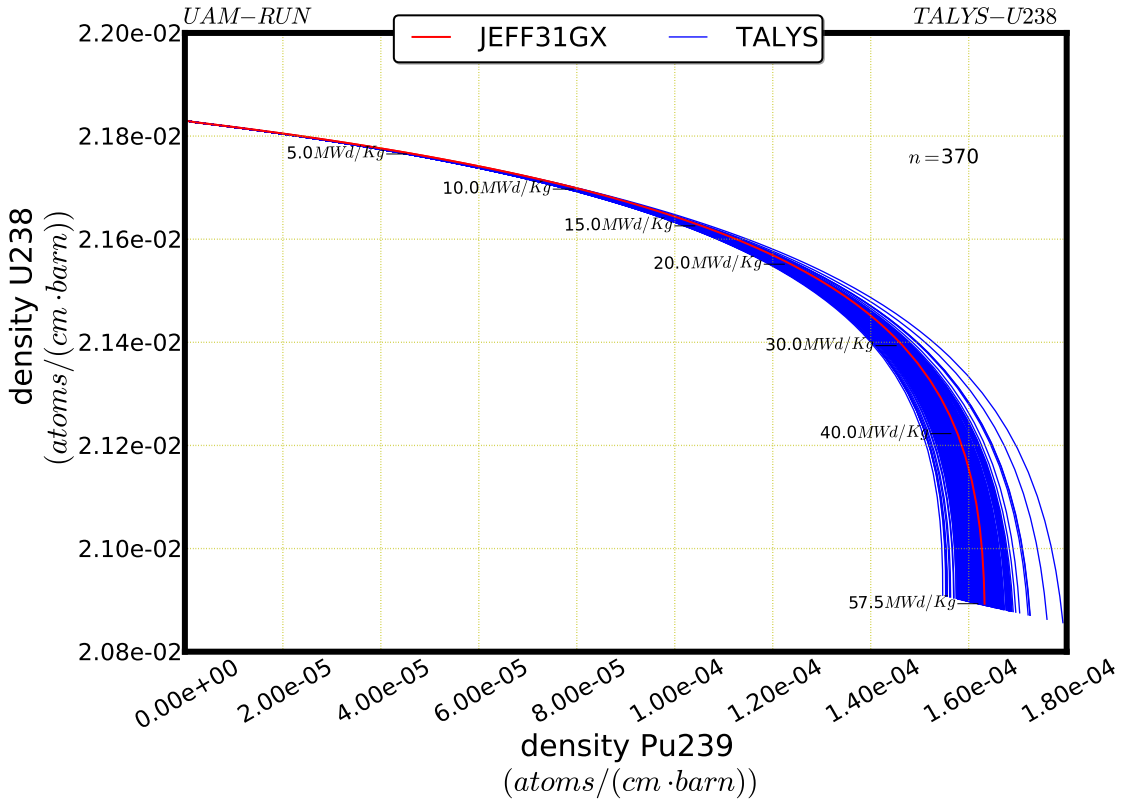

Figure 3.13: Negative correlation between ^{239}Pu density and ^{238}U density

The uncertainty of this reaction varies from 0.58 to 2% within the thermal and resonance range respectively. Provided that the flux uncertainty is much smaller and can be neglected, we can expect an uncertainty on the production reaction rate (and therefore the density uncertainty of ^{239}Pu at the start of the cycle) of roughly the same order (explaining the 1% uncertainty observed in figure 3.14).
With the build-up of the Pu isotopes, and the hardening of the flux spectrum and its increasing uncertainty as a function of time, loss by fission of ^{239}Pu results in additional correlations with the flux and perhaps other reactions. It is difficult for us at this moment to understand the constant increase in the ^{239}Pu density change uncertainty.

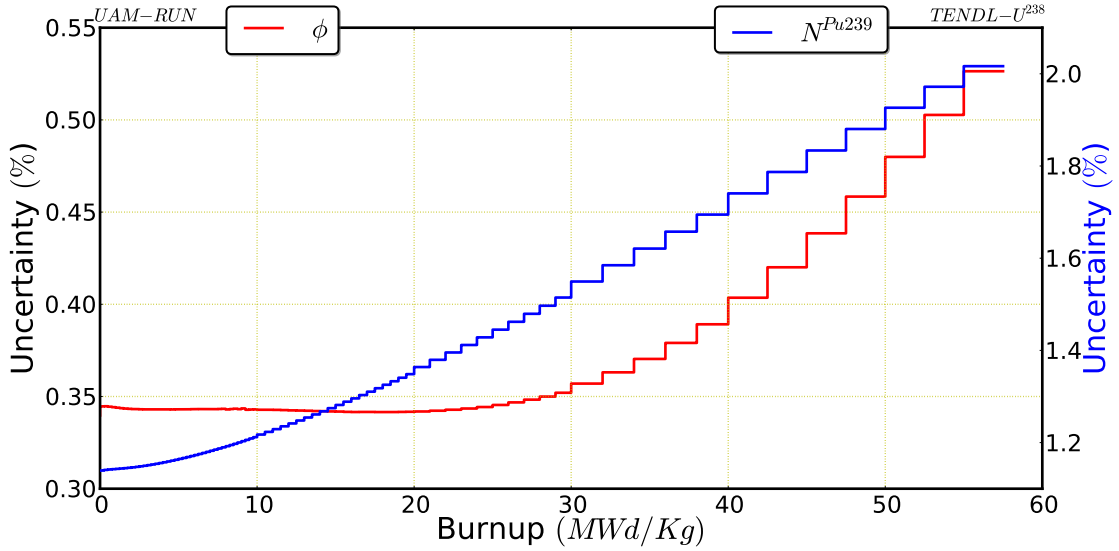

Figure 3.14: Relative uncertainity in ϕ and ^{239}Pu due at ^{238}U

3.4.2 Uncertainties due to variations in the cross sections of ^{239}Pu

Since ^{239}Pu is not present at the start of the cycle, its uncertainty density is expected to evolve with its own density (see figure 3.15). One can see that the uncertainty of the density change is larger than that of the flux. We note that the flux as well as the uncertainties of the 239Pu (n, γ) and (n, f) cross sections contribute to its density change uncertainty.

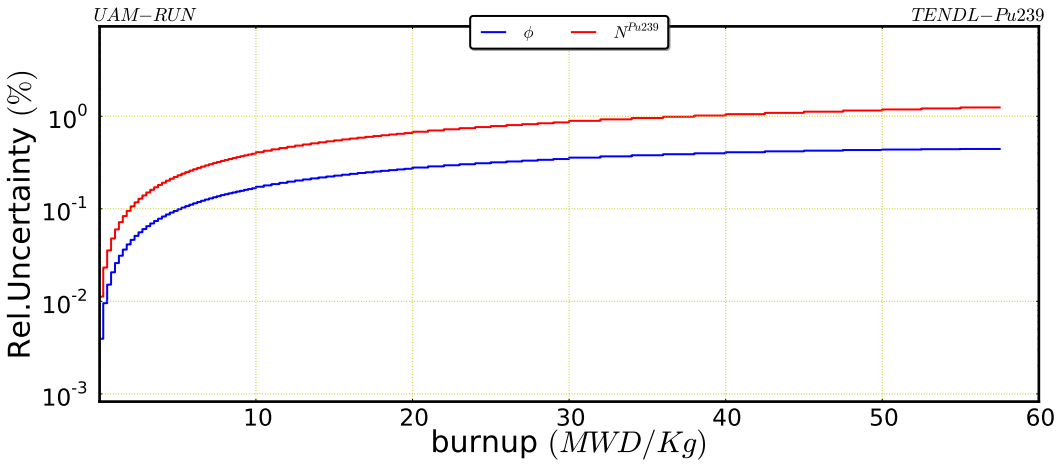

Figure 3.15: Relative uncertainity in ϕ and ^{239}Pu density due to ^{239}Pu cross section uncertainties

3.4.3 Uncertainties due to variations in the cross sections of ^{235}U

At the start of the cycle, the major contribution to the uncertainty is that of the flux uncertainty resulting from feedback due to the variations of ^{235}U. One would expect an uncertainty on the ^{239}Pu density similar to that of the flux, as shown in figure 3.16.
At the present moment, we are very surprised with the erradic behaviour of the ^{239}Pu density uncertainty. It seems to us, that the very strong reduction in the uncertainty is correlated to the

build-up of ^{239}Pu that stalled at $30MWd/kg$. This suggests a change in the one group capture and fission cross sections induced by the spectrum shift of the flux. Further comments require a more in depth analysis.

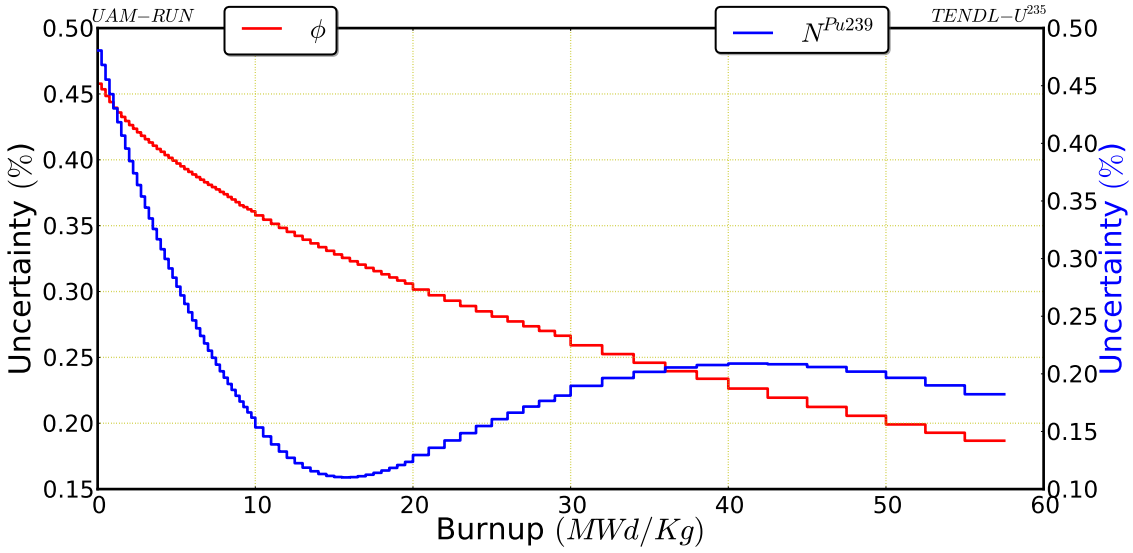

Figure 3.16: Relative uncertainity in ϕ and ^{239}Pu due at ^{235}U

Chapter 4

Final Remarks

This work has been our first attempt at uncertainty propagation using NRG's random nuclear data files. The overall results have been promising. While there exist some short comings in the quality of the data that is currently available from NRG, their methodology of sampling cross section parameters directly according to EXFOR covariances and their fashion of propagation through the evaluation using the TALYS code can lead to extremely high quality and promising results.
In particular, the multi-group covariance matrices that can be built from their data are very impressive. Traditionally, through the use of the NJOY ERRORR module, covariances can be built at a single temperature and dilution factor using perturbation theory methods to propagate through the condensation/group collapse process. In the case of the SCALE covariances, only a single set of matrices are available to be used. The advantage of the processed multi-group data set generated from NRG's ENDF files is that covariance matrices can easily be built at a requested temperature and at desired group dependent dilution factor. This eliminates much of the complications that accompany propagation through self shielding. Once the multi-group sample libraries are available, the process of construction of the matrices takes approximately half an hour on a personal PC per isotopes. One may chose to construct a matrix for each case or apply the same matrix to similar cases. Furthermore, the constructed covariances are guaranteed to satisfy the properties of covariance matrices. As shown in chapter 2, if sensitivity coefficients are calculated properly, the results predicted by use of these matrices are consistent with results of direct simulations. Naturally, the quality of the matrices will depend directly on the quality of the data provided by NRG.
Finally, given that the link between the evaluated data file and the multi group library is established (done in chapter 1 of this report), the Total Monte Carlo method of NRG provides an extremely user friendly means of propagation of the case studied. The downfall is the difficulty in understanding the results. The method is capable of producing an estimated uncertainty on any calculated parameter of interest but understanding and interpretation of the results requires access to individual reaction contributions and sensitivities which are not available if a TMC approach is chosen.

Bibliography

[1] M.B. Chadwicka, , M. Hermanb, P. Oblozinskyb, M.E. Dunnc, Y. Danond, A.C. Kahlera, D.L. Smithe, B. Pritychenkob, G. Arbanasc, R. Arcillab, R. Brewera, D.A. Brownb, f, R. Capoteg, A.D. Carlsonh, Y.S. Chom, H. Derrienc, K. Guberc, G.M. Halea, S. Hoblitb, S. Hollowaya, T.D. Johnsonb, T. Kawanoa, B.C. Kiedrowskia, H. Kimm, S. Kuniedaa, o, N.M. Larsonc, L. Lealc, J.P. Lestonea, R.C. Littlea, E.A. McCutchanb, R.E. MacFarlanea, M. MacInnesa, C.M. Mattoonf, R.D. McKnighte, S.F. Mughabghabb, G.P.A. Nobreb, G. Palmiottin, A. Palumbob, M.T. Pignic, V.G. Pronyaevi, R.O. Sayerc, A.A. Sonzognib, N.C. Summersf, P. Taloua, I.J. Thompsonf, A. Trkovj, R.L. Vogtf, S.C. van der Marckk, A. Wallnerl, M.C. Whitea, D. Wiardac, P.G. Younga *ENDF/B-VII.1 Nuclear Data for Science and Technology: Cross Sections, Covariances, Fission Product Yields and Decay Data*

[2] M.A. Kellett,O. Bersillon,R.W. Mills, *The JEFF-3.1/-3.1.1 radioactive decay data and fission yields sub-libraries* ISBN 978-92-64-99087-6

[3] K. Shibata, O. Iwamoto, T. Nakagawa, N. Iwamoto, A. Ichihara, S. Kunieda, S. Chiba, K. Furutaka, N. Otuka, T. Ohsawa, T. Murata, H. Matsunobu, A. Zukeran, S. Kamada, and J. Katakura *"JENDL-4.0: A New Library for Nuclear Science and Engineering,* J. Nucl. Sci. Technology

[4] D. Rochman and A.J. Koning. *TENDL-2011: TALYS-based Evaluated Nuclear Data Library*, submitted to the PHYSOR-2012 conference.

[5] Artem Yankov, Makus Kleis, Marhew A. Jesse, WInfried Zwermann, Kiril Velkov, Andreas Pautz, Benjamin Collins, Thomas Downar, *Comparison of XSUSA and 'TWO-STEP' aproaches for full-core uncertainty quantification'*, Physhor 2012, Knoxville, Tenessee, USA, April 1520,2012

[6] Ball, Matthew R., *"Uncertainty Analysis In Lattice Reactor Physics Calculations"* (2012). Open Access Dissertations and Theses. Paper 6565

[7] Emanuele Autino*Parametric study in the generation IV reactors fuel evolution*

[8] Members of the Cross Sections Evaluation Working Group,*ENDF-6 Formats Manual*, National Nuclear Data Center Brookhaven National Laboratory. CSEWG Document ENDF-102 Report BNL-90365-2009

[9] S.F. Mughabghad and D.I. Garber, *Neutron, Cross sections, Volume I, Resonance Parameters* June 1973

[10] *Evaluated Nuclear Data File (ENDF)* Database Version of June 15, 2012

[11] Lane A, Lynn J, *Fast neutron capture below 1 MeV: the cross sections for* ^{238} *U and* ^{232}*Th* Proceedings of the Physics Society (London) A 70(5)

[12] A.J. Koning and D. Rochman. *Towards sustainable nuclear energy: Putting nuclear physics to work*, Annals of Nuclear Energy, 35:2024, 2008.

[13] A. Koning, S. Hilaire, M.C. Duijvestijn, *Talys1.0 Preceedings of the international conference on nuclear data for science and technology* April 26-30, 2010, Jeju, Korea, Journ. of Korean Phys.

[14] D. Rochman and A.J. Koning. *Propagation of 235,236,238U and 239Pu nuclear data uncertainties for a typical PWR fuel element*, accepted in Nucl. Technology, October 2011.

[15] [reference burnup paper above]

[16] Los Alamos, *The NJOY nuclear data processing. Version 91* LA-12740-M

[17] *WIMS-D library update : final report of a coordinated research project* Vienna , International Atomic Energy Agency, 2007.

[18] A. Hebert, G. Marleau, *Generalization of the Stamm'ler Method for the Self-Shielding of Resonant Isotopes in Arbitrary Geometries*, Journal of Nuclear Science and Engineering, 1991(18)

[19] *Benchmark for Uncertainty Analysis in Modeling (UAM) for Design, Operation, and Safety Analysis of LWRs*, Nuclear Energy Agency, NEA/NSC/DOC(2012)

[20] G. Marleau, R. Roy and A. Hebert, *DRAGON: A Collision Probability Transport Code for Cell and Supercell Calculations*, Report IGE-157, Institut de genie nucleaire,École Polytechnique de Montréal, Montreal, Québec (1994)

[21] Donald L. Smith, PhD *Probability, Statistics, and Data Uncertainties in Nuclear Science and Technology* 1991

[22] L.N. Usachev, *Perturbation Theory for the Breeding nd for other number ratios pertaining to various reactor processes*, Journal of Nuclear Energy Parts A/B (1964), 571(18)

[23] Bidaud, A., Marleau, G., Noblat E., *Nuclear Data Uncertainty Analysis Using the Coupling of DRAGON With SUSD3D*, International Conference on Mathematics, Computational Methods and Reactor Physics 2009, v. 4, p. 2348-2357.

Item ID: 300025 / ISBN: 0-89448-036-7

[24] D. Cacuci, *Handbook of Nuclear Engineering*

[25] F. Perrin. Prise en compte des données expérimentales dans les modèles de prévision de la durée de vie des structures. Thèse de doctorat, Université Blaise Pascal Clermont-Ferrand II, 2008.

Appendix A

Comparison of uncertainties between TALYS, JENDL-4 & SCALE

A.1 Comparison of the Uncertainties from JENDL-4,SCALE and TALYS

A.1.1 ^{238}U cross section uncertainties for the TALYS generated covariances

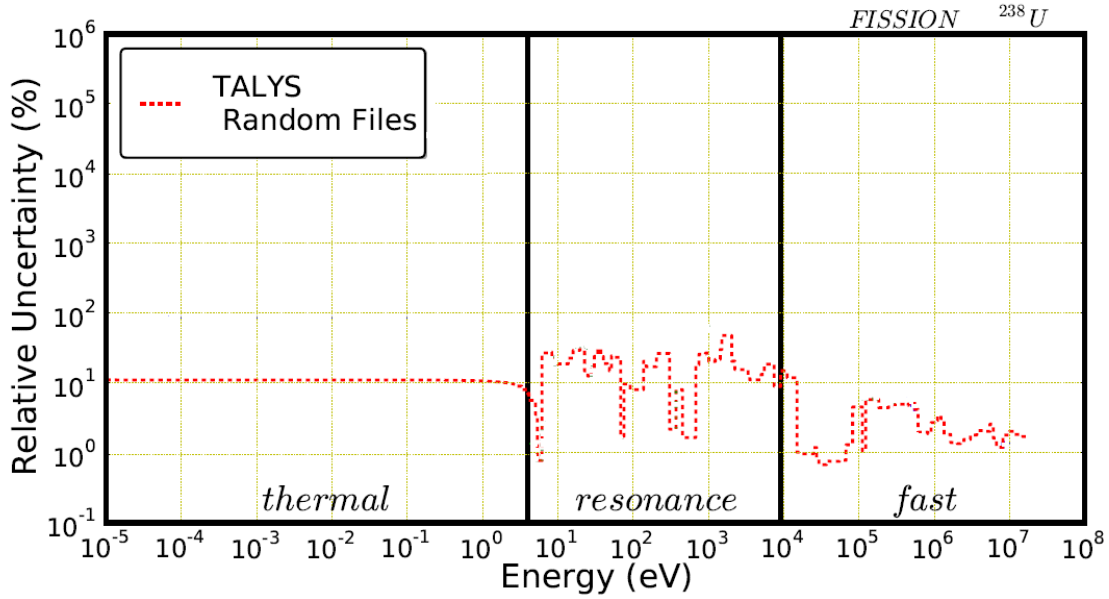

Figure A.1: ^{238}U fission cross section uncertainty for the TALYS generated covariances

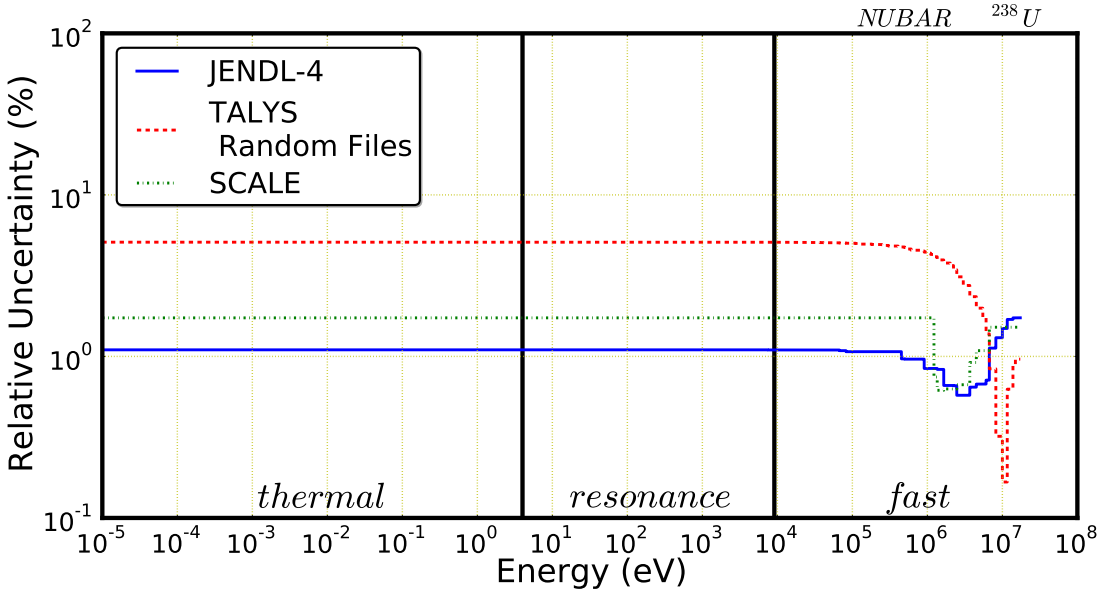

Figure A.2: ^{238}U nubar uncertainty for the TALYS generated covariances, covariances of SCALE-6, and JENDL-4

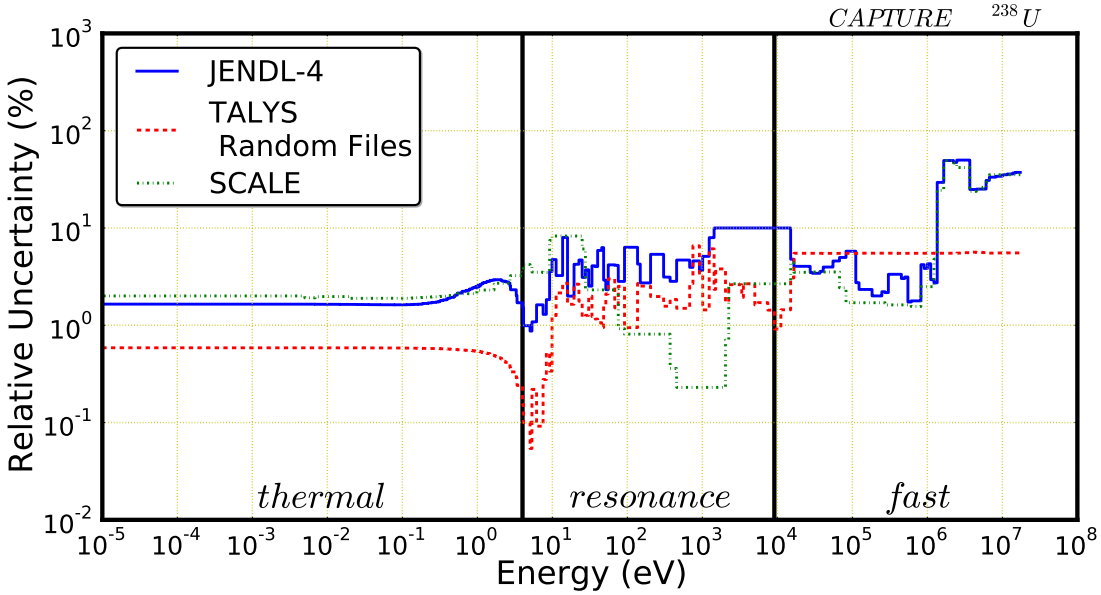

Figure A.3: ^{238}U capture cross section uncertainty for the TALYS generated covariances, covariances of SCALE-6, and JENDL-4

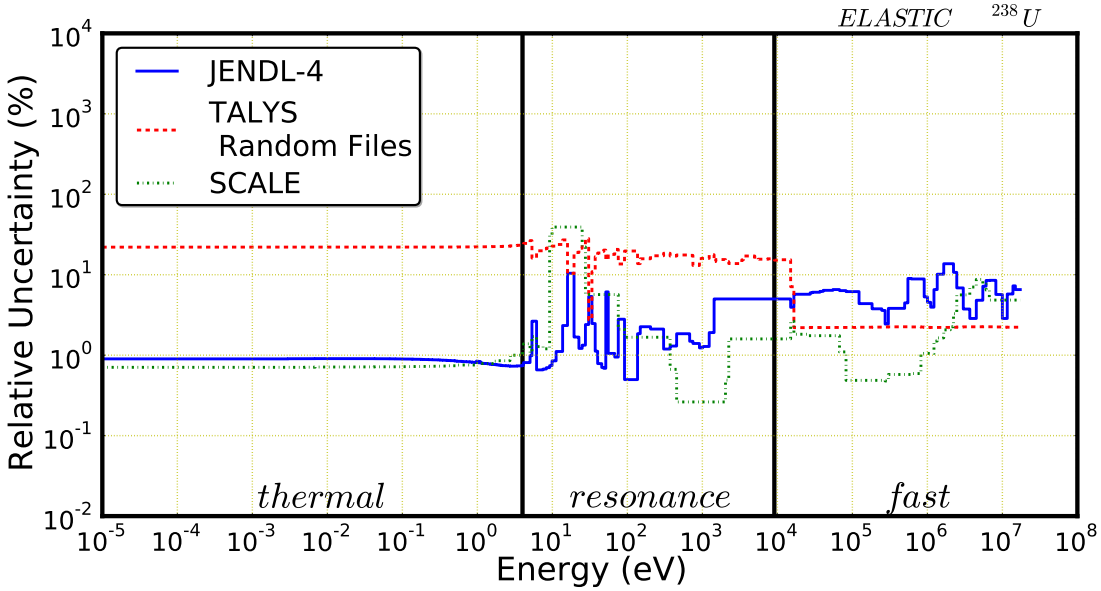

Figure A.4: ^{238}U elastic cross section uncertainty for the TALYS generated covariances, covariances of SCALE-6, and JENDL-4

A.1.2 ^{238}U cross section uncertainties for the TALYS generated covariances

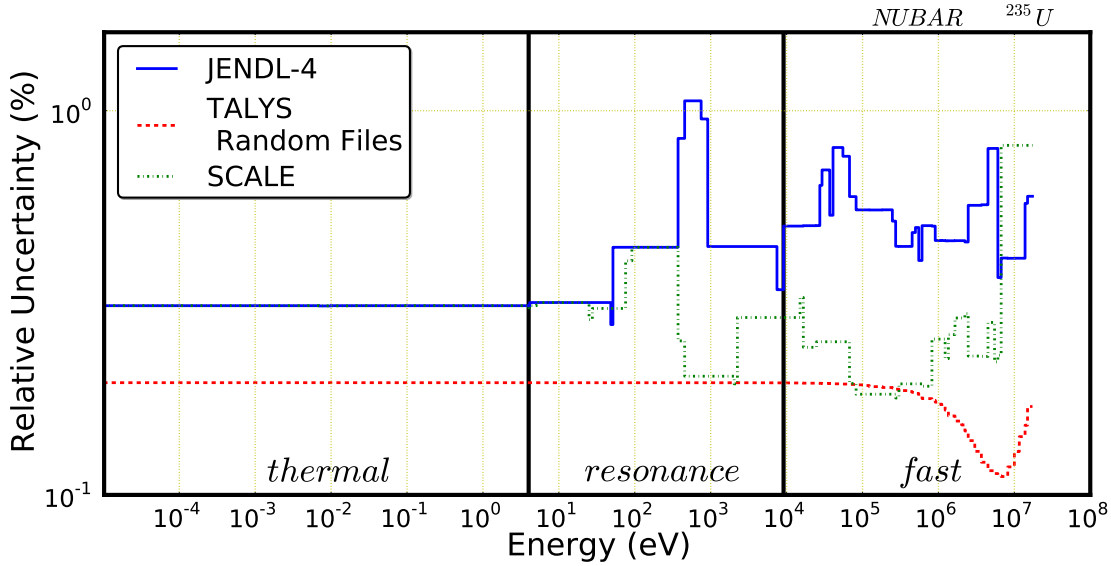

Figure A.5: ^{235}U $\bar{\nu}$ uncertainties for the TALYS generated covariances, covariances of SCALE-6, and JENDL-4

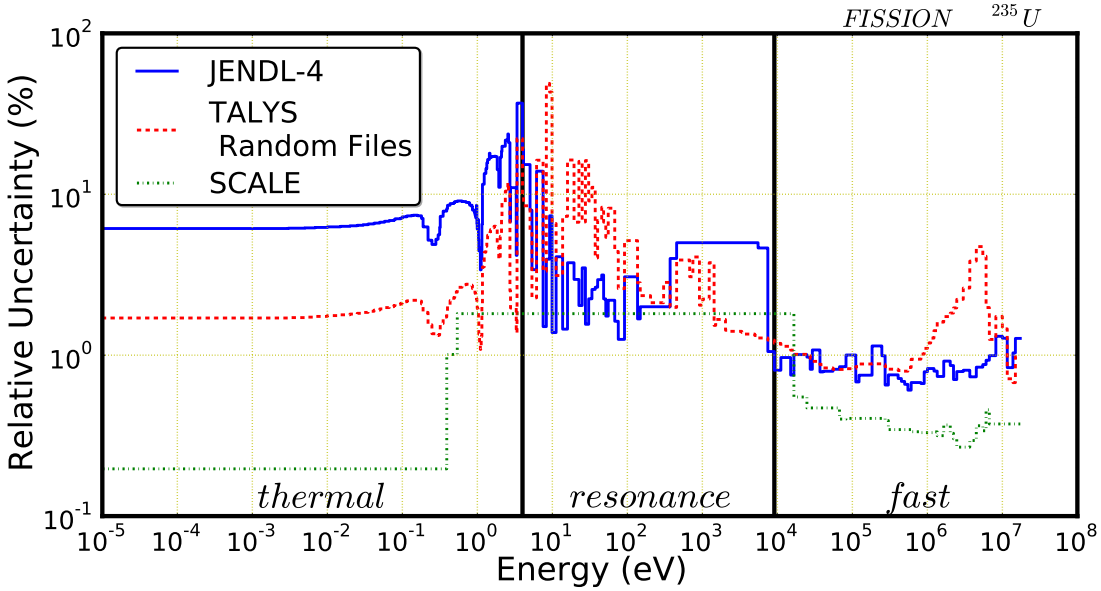

Figure A.6: ^{235}U fission cross section uncertainty for the TALYS generated covariances, covariances of SCALE-6, and JENDL-4

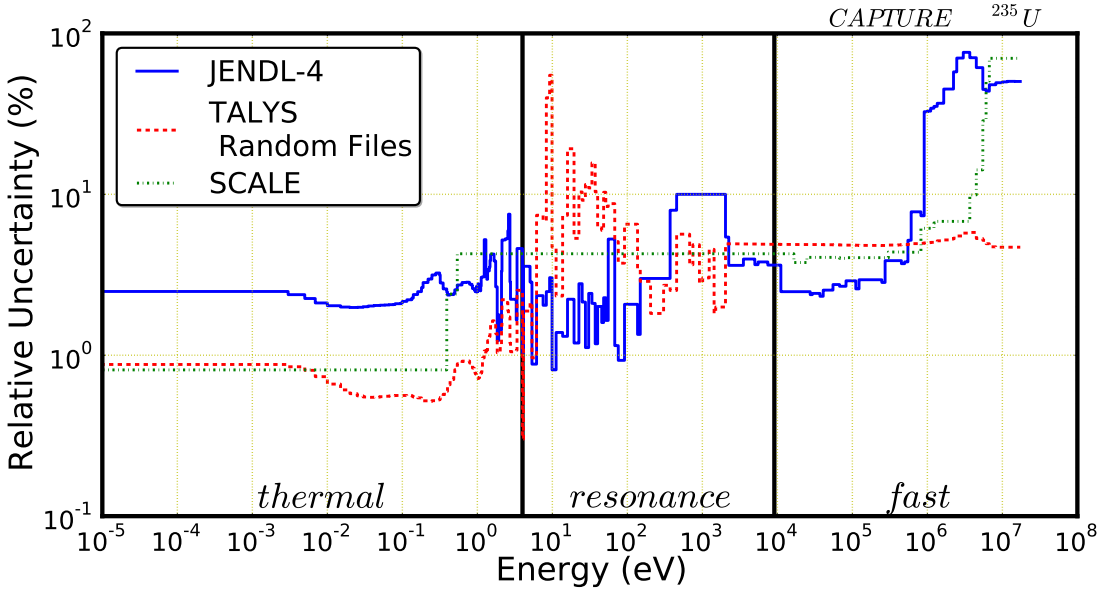

Figure A.7: ^{235}U capture cross section uncertainty for the TALYS generated covariances, covariances of SCALE-6, and JENDL-4

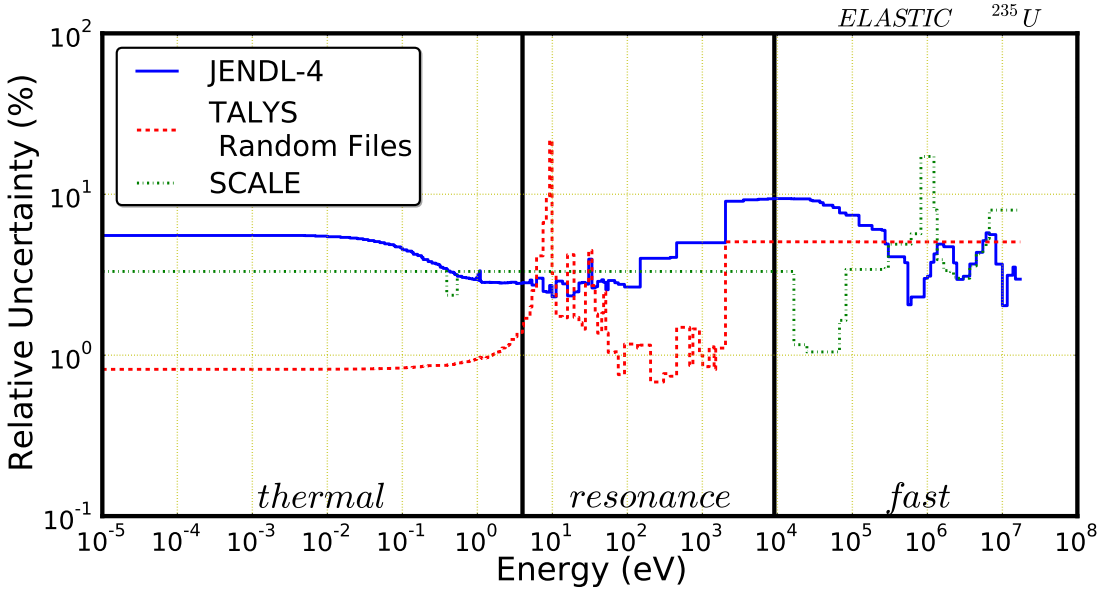

Figure A.8: ^{235}U elastic cross section uncertainty for the TALYS generated covariances, covariances of SCALE-6, and JENDL-4

A.1.3 Correlation matrices

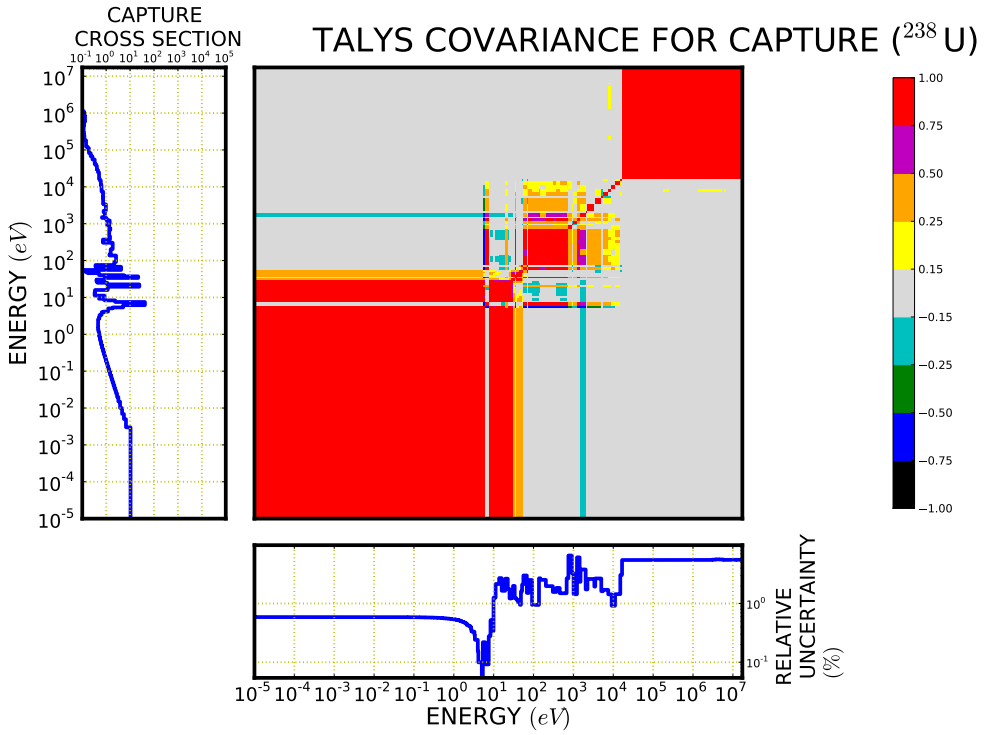

Figure A.9: Correlation matrix for ^{238}U TALYS for capture

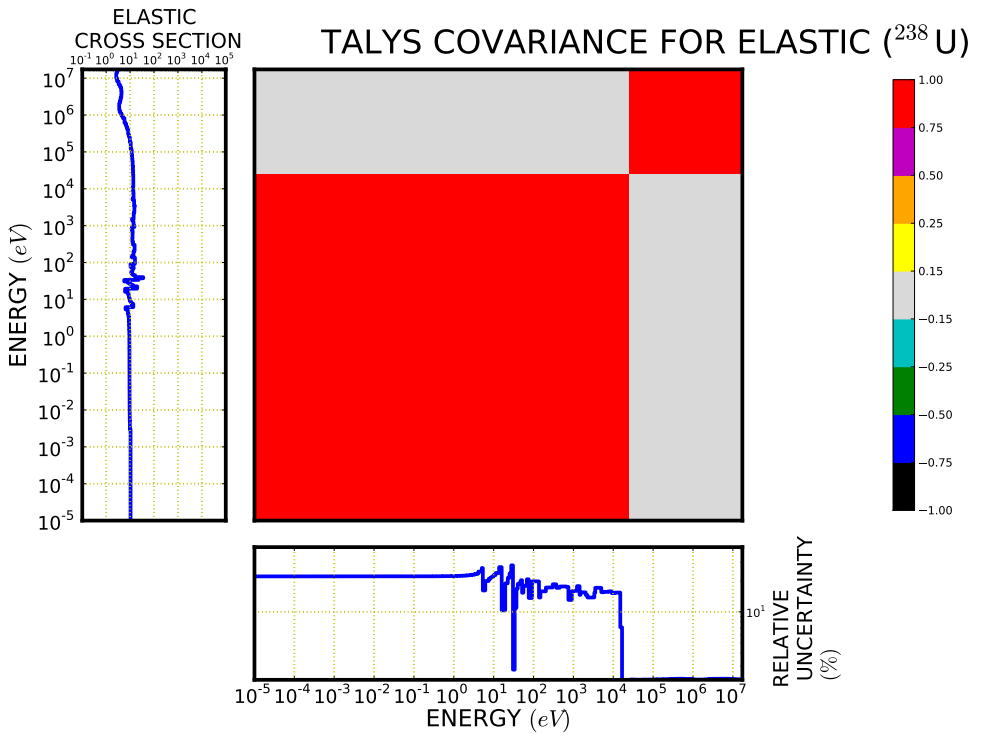

Figure A.10: Correlation matrix for ^{238}U TALYS elastic

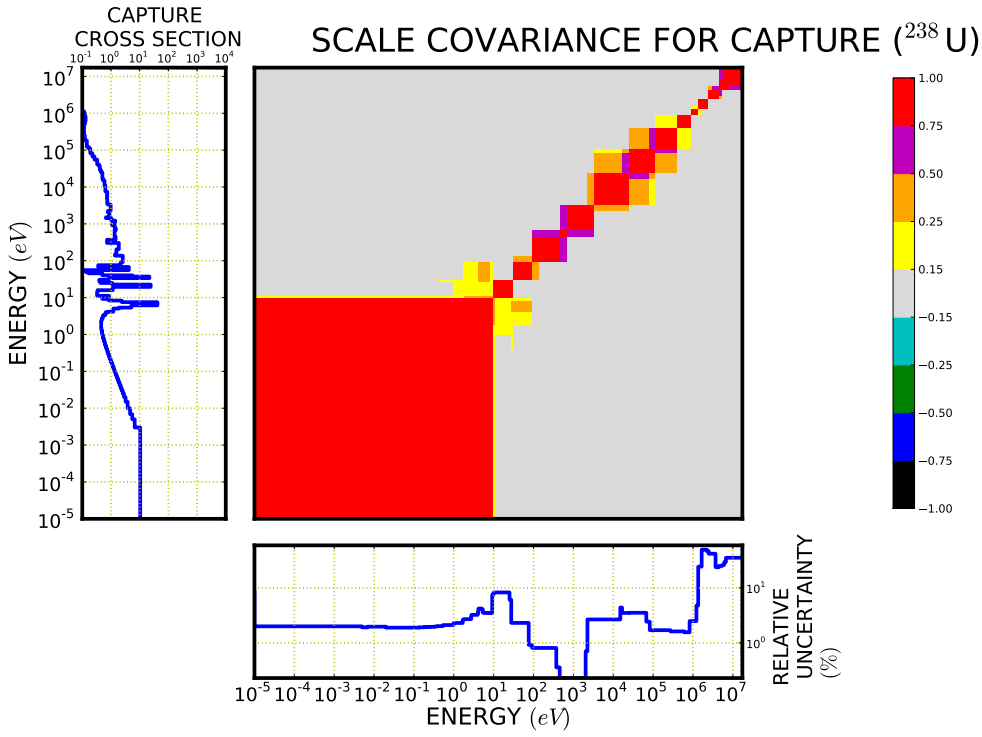

Figure A.11: Correlation matrix for ^{238}U SCALE capture

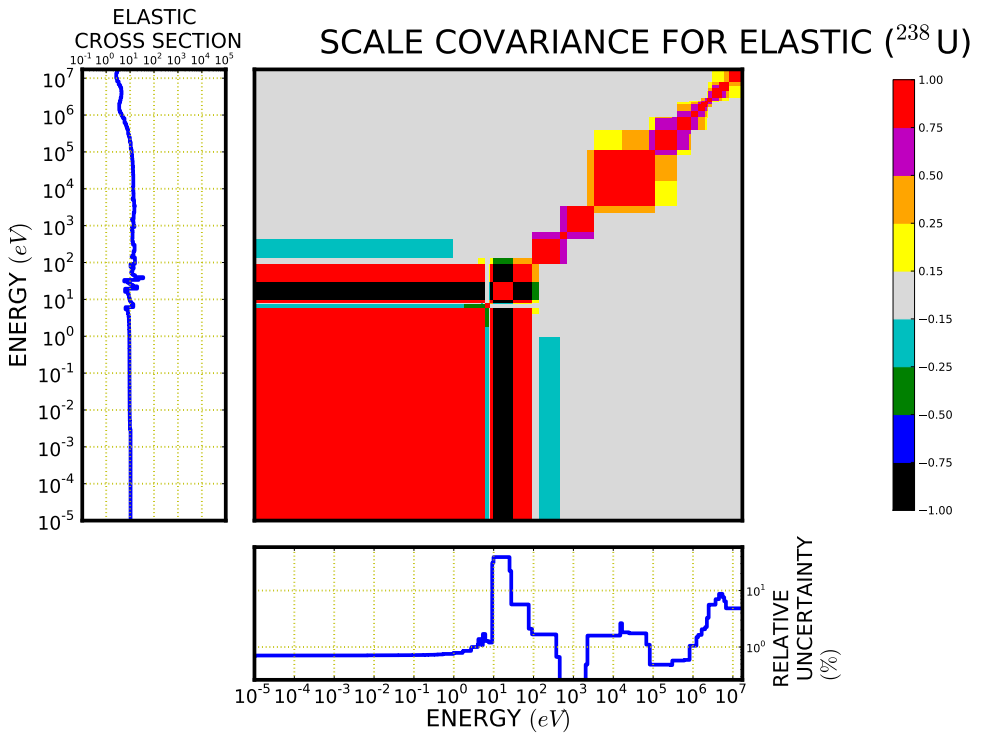

Figure A.12: Correlation matrix for ^{238}U SCALE elastic

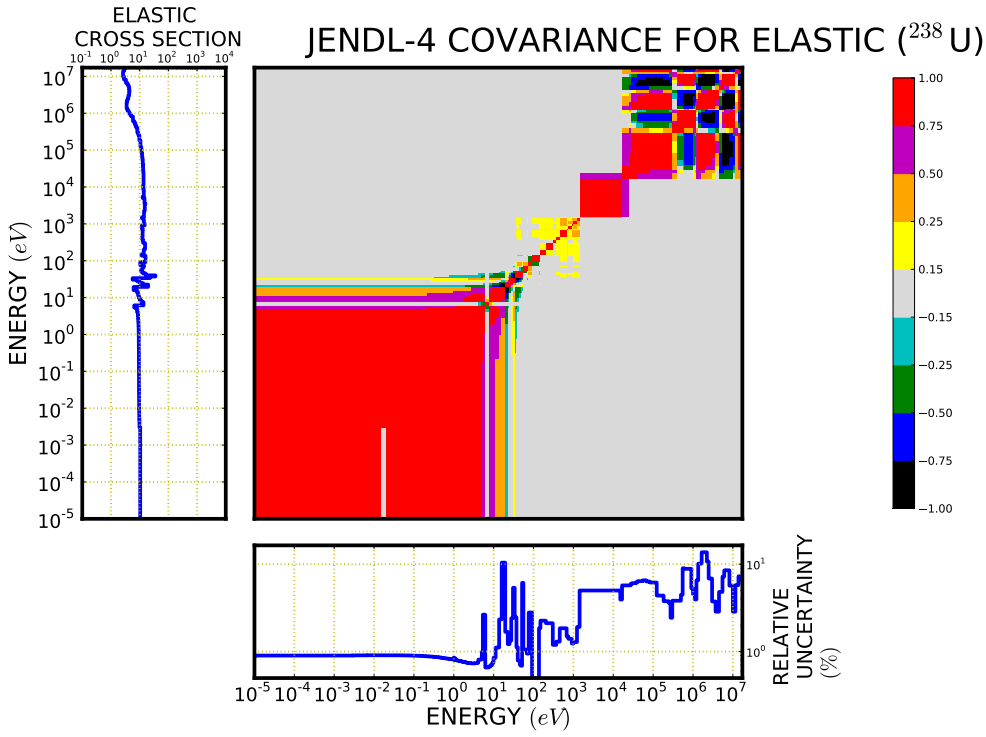

Figure A.13: Correlation matrix for ^{238}U JENDL-4 elastic

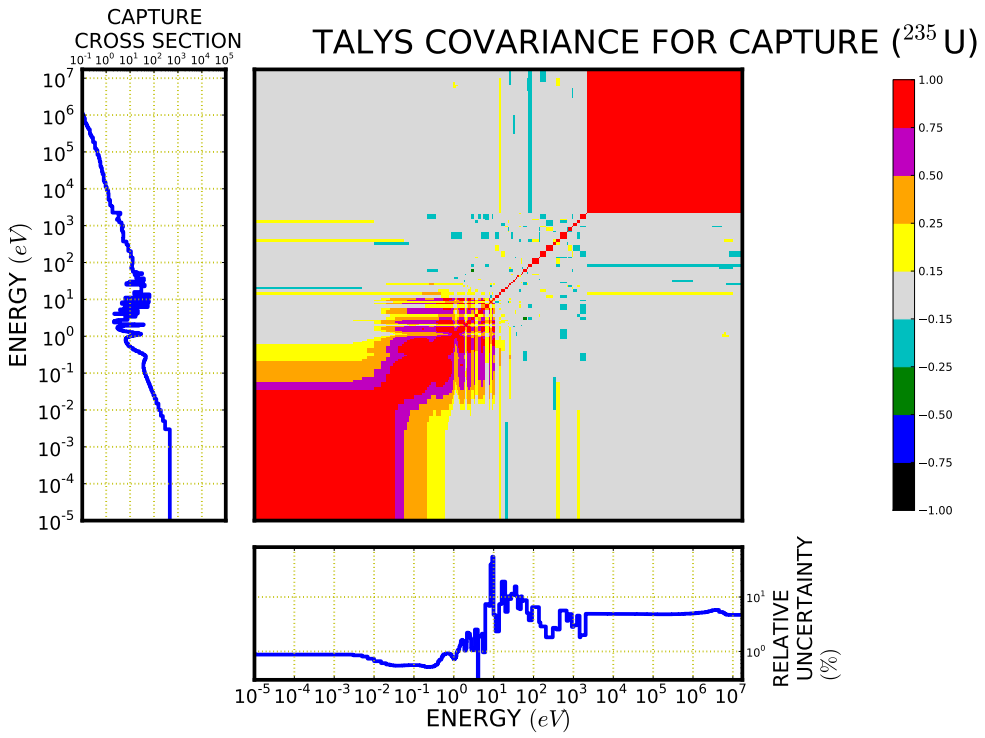

Figure A.14: Correlation matrix for ^{235}U TALYS for capture

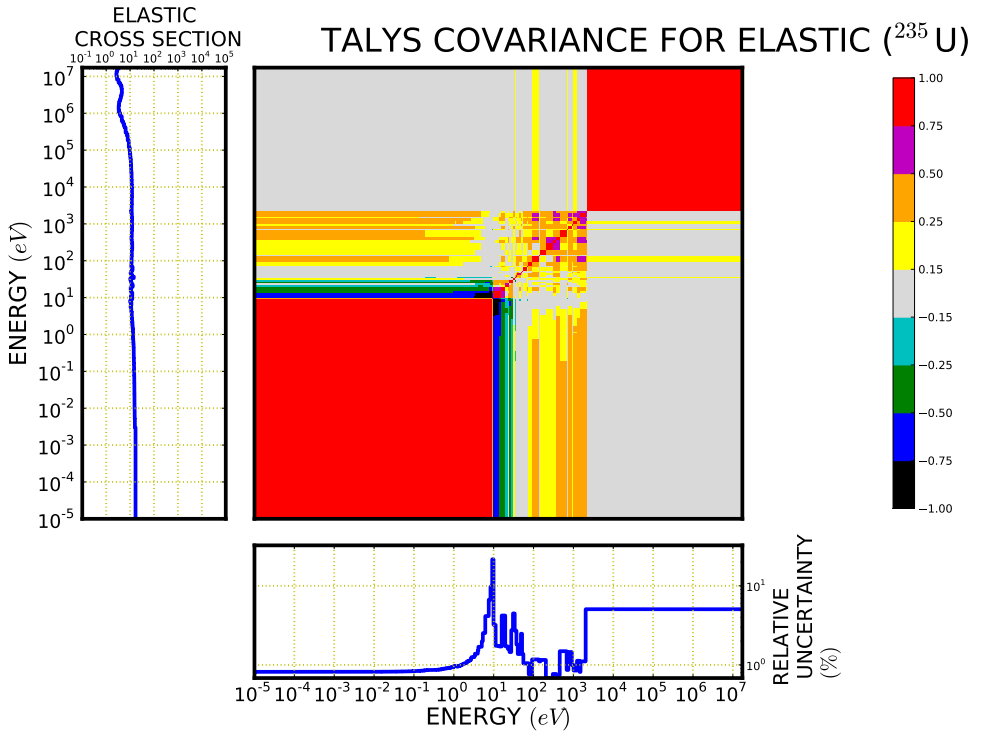

Figure A.15: Correlation matrix for ^{235}U TALYS elastic

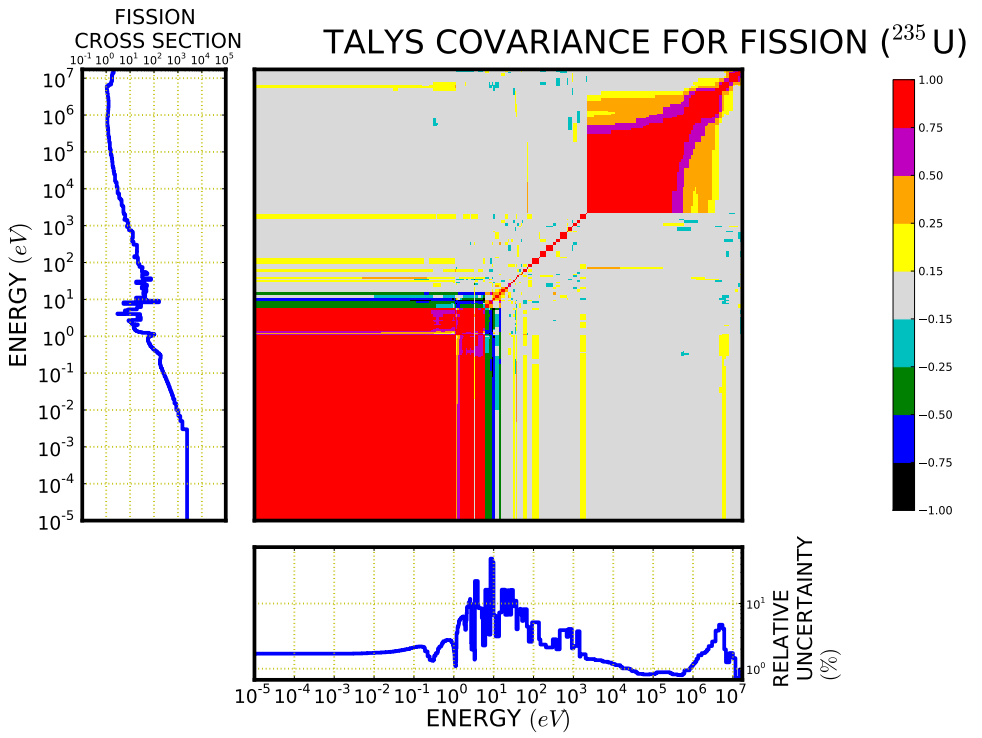

Figure A.16: Correlation matrix for ^{235}U TALYS fission

SCALE

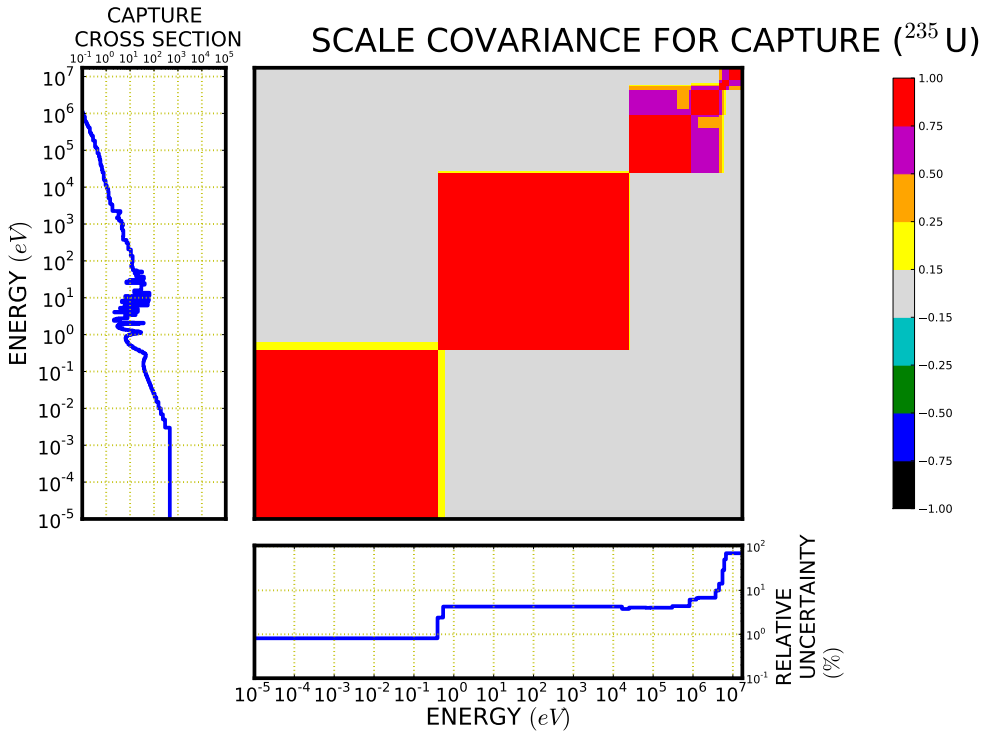

Figure A.17: Correlation matrix for ^{235}U SCALE for capture

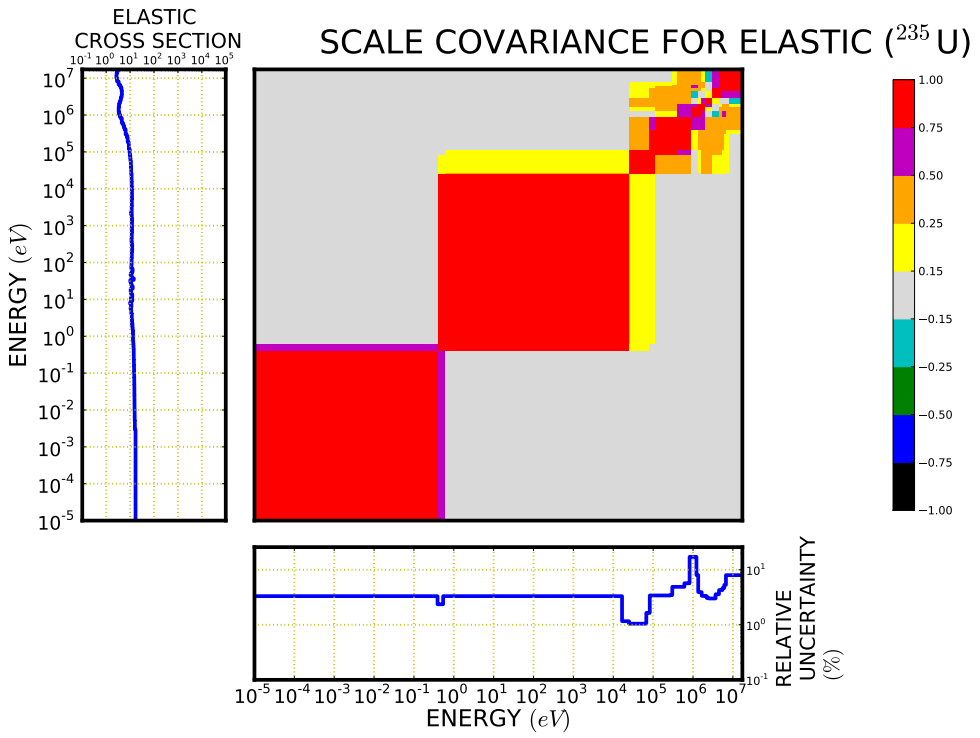

Figure A.18: Correlation matrix for ^{235}U SCALE elastic

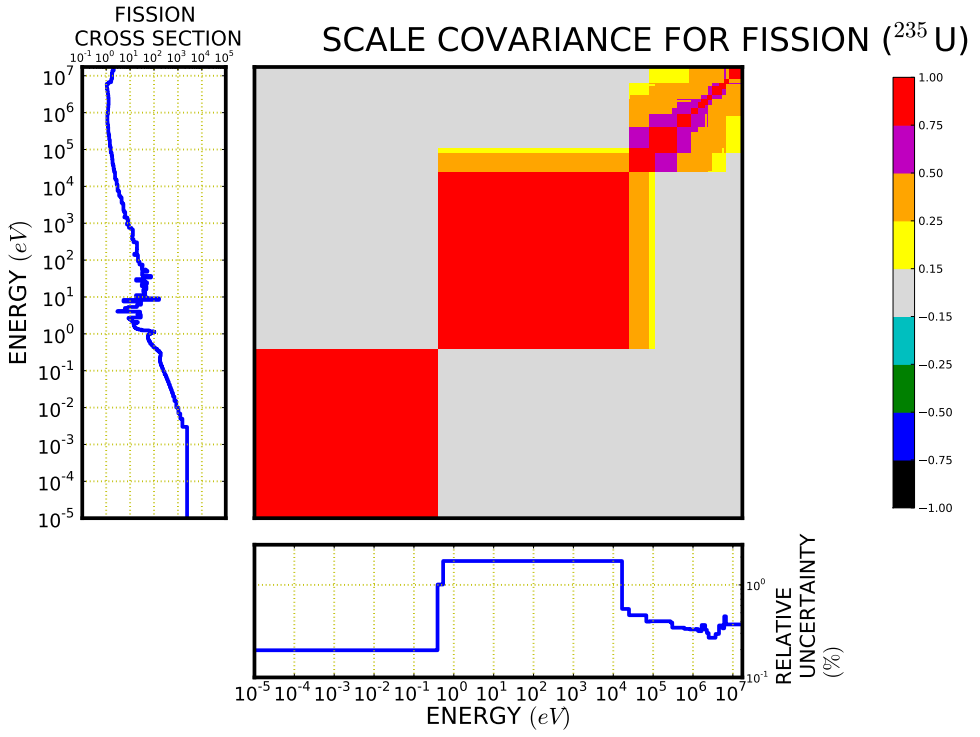

Figure A.19: Correlation matrix for ^{235}U SCALE fission

JEDNL

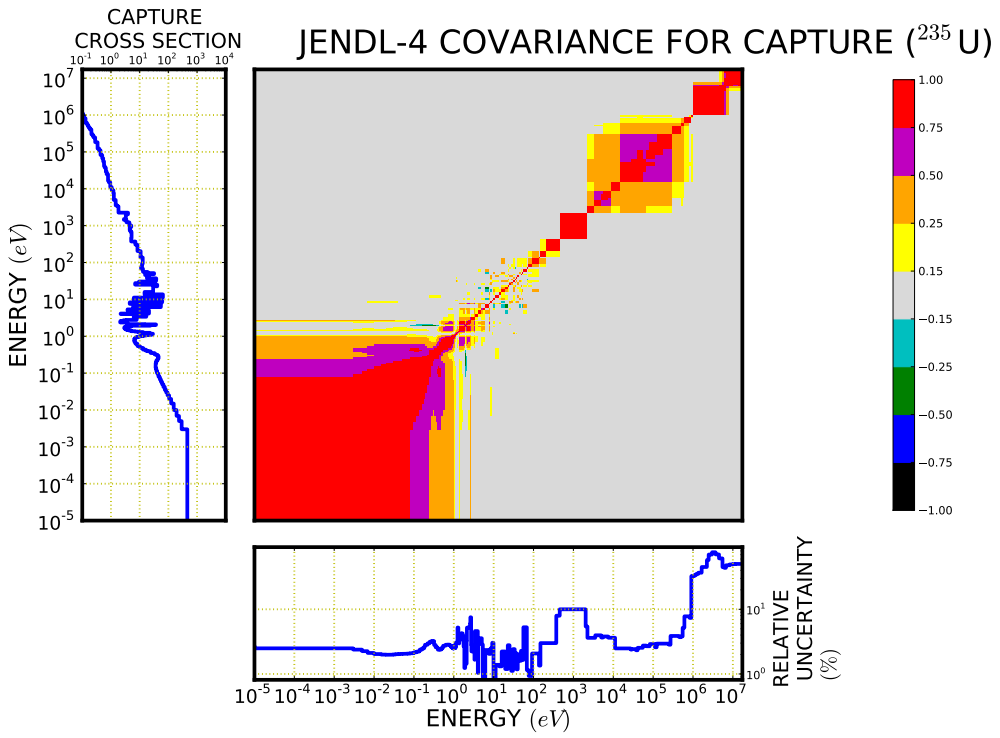

Figure A.20: Correlation matrix for ^{235}U JENDL-4 for capture

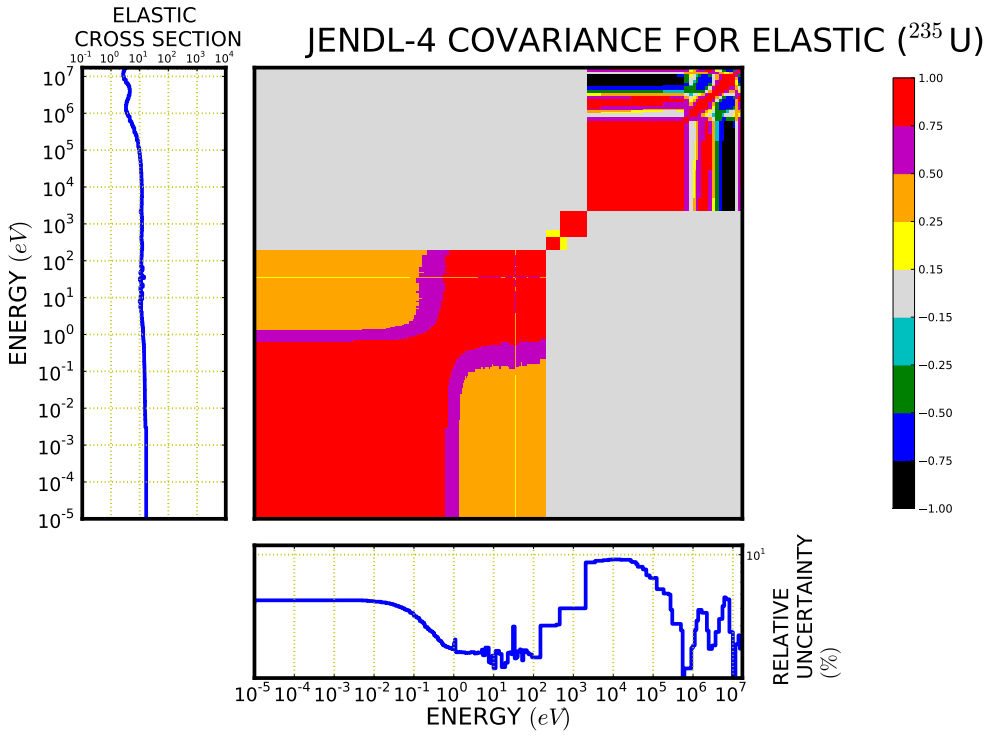

Figure A.21: Correlation matrix for ^{235}U JENDL-4 elastic

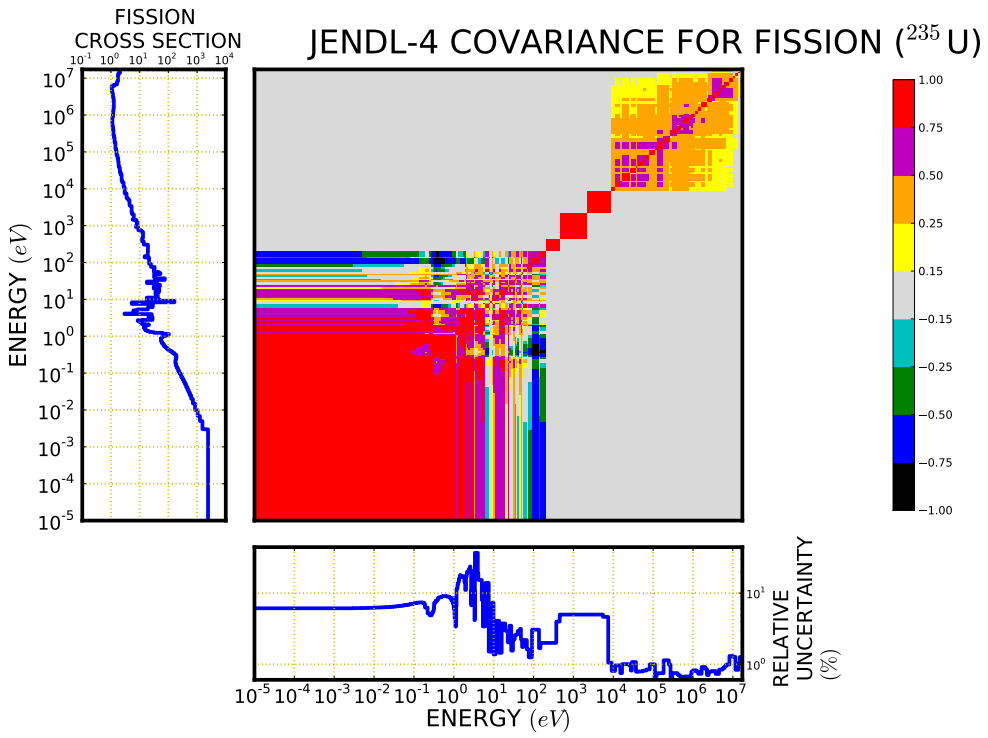

Figure A.22: Correlation matrix for ^{235}U JENDL-4 fission

Appendix B

Input NJOY

A standard NJOY input is taken from that available on the WLUP website. Note that for each random file, the scattering radius should be replaced with that available in the random file.

Appendix C

Validation for WIMSR.PY and WIMSLIB.py

Different version and differets moduls of NJOY (purr and unrsr) are used to process the evulated data. The WIMS output from NJOY is read by WIMSR.PY and replaced with WIMSLIB.PY in the jeff31gx library. For ^{1}H,^{2}He,^{12}C and ^{16}0 P1 matrix hace been replaced.Mixtures as Cd, Sn or Ni are created with WILLIE. The modificated libraries are used to launch DRAGON.

Table C.1: K_{eff} and error for the isotopes studied

Jeff31gx	case1		case2		case3	
mat	k_{eff}	porc	k_{eff}	porc	k_{eff}	porc
125	1,44806862	-0,00532669	1,33326769	0,00234231	1,42083478	0,00245835
128	1,44799149	0,00000000	1,33329892	0,00000000	1,42086971	0,00000000
228	1,44799149	0,00000000	1,33329892	0,00000000	1,42086971	0,00000000
600	1,44799149	0,00000000	1,33329892	0,00000000	1,42086971	0,00000000
825	1,44798875	0,00018923	1,33330512	-0,00046501	1,42087126	-0,00010909
825	1,44799089	0,00004144	1,33330488	-0,00044701	1,42087138	-0,00011753
1625	1,44799149	0,00000000	1,33329892	0,00000000	1,42086971	0,00000000
2525	1,44799149	0,00000000	1,33329892	0,00000000	1,42086971	0,00000000
si	1,44799149	0,00000000	1,33329892	0,00000000	1,42086971	0,00000000
s	1,44799149	0,00000000	1,33329892	0,00000000	1,42086971	0,00000000
cr	1,44799197	-0,00003315	1,33329892	0,00000000	1,42086971	0,00000000
fe	1,44799137	0,00000829	1,33329892	0,00000000	1,42086971	0,00000000
ni	1,44799089	0,00004144	1,33329892	0,00000000	1,42086971	0,00000000
Zr	1,44799149	0,00000000	1,33330250	-0,00026851	1,42087305	-0,00023507
mo	1,44799149	0,00000000	1,33329892	0,00000000	1,42086971	0,00000000
cd	1,44799149	0,00000000	1,33329892	0,00000000	1,42086971	0,00000000
sn	1,44799149	0,00000000	1,33331907	-0,00151129	1,42088795	-0,00128372
6431	1,44799149	0,00000000	1,33329892	0,00000000	1,42086971	0,00000000
6434	1,44799149	0,00000000	1,33329892	0,00000000	1,42086971	0,00000000
6437	1,44799149	0,00000000	1,33329892	0,00000000	1,42086971	0,00000000
6440	1,44799149	0,00000000	1,33329892	0,00000000	1,42086971	0,00000000
6443	1,44799149	0,00000000	1,33329892	0,00000000	1,42086971	0,00000000
9228	1,44799173	-0,00001657	1,33329856	0,00002700	1,42086959	0,00000845
9237	1,44803357	-0,00290609	1,33330643	-0,00056326	1,42087901	-0,00065453
9438	1,44797313	0,00126796	1,33329892	0,00000000	1,42086971	0,00000000
9440	1,44799173	-0,00001657	1,33329892	0,00000000	1,42086971	0,00000000
9443	1,44798803	0,00023895	1,33329892	0,00000000	1,42086971	0,00000000
9946	1,44799149	0,00000000	1,33329892	0,00000000	1,42086959	0,00000845
9543	1,44830203	-0,02144626	1,33329892	0,00000000	1,42086971	0,00000000
4234	1,44800103	-0,00065884	1,33329892	0,00000000	1,42086971	0,00000000
9434	1,44799161	-0,00000829	1,33329892	0,00000000	1,42086971	0,00000000

Isotopes availables are included in a empty library and library from TENDL data have been created.